Monthly Notices
of the
ROYAL ASTRONOMICAL SOCIETY

MNRAS **489,** 1304–1320 (2019)
Advance Access publication 2019 August 16

doi:10.1093/mnras/stz2165

New β Cep pulsators discovered with *K2* space photometry

S. Burssens [1]★ D. M. Bowman [1] C. Aerts [1,2] M. G. Pedersen,[1] E. Moravveji[1] and B. Buysschaert[1,3]

[1]*Instituut voor Sterrenkunde, KU Leuven, Celestijnenlaan 200D, B-3001 Leuven, Belgium*
[2]*Department of Astrophysics, IMAPP, Radboud University Nijmegen, NL-6500 GL Nijmegen, the Netherlands*
[3]*LESIA, Observatoire de Paris, PSL Research University, CNRS, Sorbonne Universités, UPMC Univ. Paris 06, Univ. Paris Diderot, Sorbonne Paris Cité, 5 place Jules Janssen, F-92195 Meudon, France*

Accepted 2019 July 31. Received 2019 July 11; in original form 2019 February 11

ABSTRACT

We present the discovery of three new β Cep pulsators, three new pulsators with frequency groupings, and frequency patterns in a B3Ib star, all of which show pulsations with frequencies as high as about 17 d^{-1}, with *K2* space mission photometry. Based on a Fourier analysis and iterative pre-whitening, we present a classification and evaluate the potential for asteroseismic modelling. We include the lists of pulsation frequencies for three new β Cep pulsators, CD-28 12286, CD-27 10876, LS 3978, and additional pulsation mode frequencies for the known β Cep pulsator HD 164741. In addition, we characterize the regular frequency spacing found in the new pulsator HD 169173, and discuss its origin. We place the newly discovered variables in a colour–magnitude diagram using parallaxes from *Gaia* DR2 (second data release), showcasing their approximate location in the massive star domain. The identified frequency lists of these multiperiodic pulsators are a good starting point for future forward seismic modelling, after identification of at least one pulsation frequency from high-resolution time-series spectroscopy and/or multicolour photometry.

Key words: asteroseismology – techniques: photometry – stars: individual: CD-28 12286, CD-27 10876, LS 3978, HD 164741, HD 169173 – stars: massive.

1 INTRODUCTION

Despite massive stars not being as common as lower mass stars, they are the metal factories of our Universe enriching their surroundings by means of stellar winds and supernovae explosions. Massive star physics such as fast rotation, mass loss, and binarity complicate stellar modelling and evolutionary predictions (Maeder 2009). Consequently, the interior physics of massive stars remains poorly constrained: specifically the shape of core overshooting (Moravveji et al. 2015, 2016; Salaris & Cassisi 2017; Pedersen et al. 2018), angular momentum transport (Aerts, Mathis & Rogers 2019b), and chemical mixing are all phenomena of which we have limited observationally motivated understanding. In the last decade increasing efforts have been made to understand these stars by means of asteroseismology. This provides a powerful way to study both the global and local physics of the star, see Aerts, Christensen-Dalsgaard & Kurtz (2010) for an extended overview of this method.

The advent of space missions such as *CoRoT* (Auvergne et al. 2009), *Kepler* (Borucki et al. 2010), *K2* (Howell et al. 2014), and more recently *TESS* (Ricker et al. 2014), heralded a new age in the asteroseismology of OB-type massive stars. The high duty cycles and long time bases uninterrupted space photometry are the necessary data properties for the asteroseismology community. Pulsation frequencies can be extracted via iterative pre-whitening (see Lenz & Breger 2004; Degroote et al. 2009; Pápics et al. 2012; Bowman 2017), and if regularities in the extracted pulsation mode frequencies are detected, inference is possible of the interior of the star (Van Reeth, Tkachenko & Aerts 2016; Pápics et al. 2017; Van Reeth et al. 2018). Pulsations in early-type main-sequence stars generally occur in two frequency regimes: the low-frequency gravity modes and the high-frequency pressure modes. Gravity (g) modes are standing waves for which the dominant restoring force is buoyancy. These probe the near-core region of a star. Pressure (p) modes are standing sound waves for which the restoring force is the pressure force, and predominantly probe the stellar envelope. Each wave is characterized by three numbers: n for the radial order, ℓ for the spherical degree, and m for the azimuthal order (Aerts et al. 2010). In the case of high radial orders ($|n| >> \ell$) in a chemically homogeneous non-rotating star, p and g modes are equally spaced in frequency and period, respectively, according to the asymptotic theory of stellar oscillations (Tassoul 1980). Deviations caused by chemical composition (μ-) gradients or rotation, lead to dips (for

★ E-mail: siemen.burssens@kuleuven.be

the former) or a slope (for the latter) in the g-mode period spacing pattern (Miglio et al. 2008; Bouabid et al. 2013; Van Reeth et al. 2015; Ouazzani et al. 2017).

A recent example of using forward seismic modelling that exploited g-mode period spacing patterns in a Slowly Pulsating B star (SPB) is Moravveji et al. (2016), who argued that the g modes in KIC 7760680 indicate moderate rotation, convective core overshooting as well as diffusive mixing in the radiatively stratified layers of the envelopes. Similarly, by modelling observed g-mode spacing patterns, Pápics et al. (2017) and Szewczuk & Daszyńska-Daszkiewicz (2018) were able to measure the near-core rotation in a selection of SPBs, and constrain interior chemical mixing using *Kepler* mission data. As discussed in detail by Pedersen et al. (2018), modelling g-mode period spacing patterns can yield information about the specific shape and size of the overshooting. In Buysschaert et al. (2018b), it was shown that convective overshoot suppression by large-scale magnetic fields can be inferred by modelling g modes, for HD 43317. The power of using g-mode period spacing patterns for stellar modelling for massive stars, is extensively discussed in Aerts et al. (2018a).

Additionally, *CoRoT* data have contributed to the advancement of asteroseismology of upper main sequence pulsators. The origin of the observed oscillations in the only known β Cephei (β Cep) star observed by *CoRoT*, V1449 Aquilae, has been extensively discussed in Belkacem et al. (2009), Degroote et al. (2009), and Aerts et al. (2011). A few massive O-stars were also observed, Degroote et al. (2010) noted regular frequency spacings in the young O-type binary HD 46149 and attributed it to stochastic excitation in the subsurface convective zones. A detailed asteroseismic study by Briquet et al. (2011) on the O9V star HD 46202 demonstrated that the excitation of pulsations in massive stars is still not globally understood. A similar conclusion was obtained by Blomme et al. (2011) for three hot O-type stars where the frequency spectrum is dominated by astrophysical red noise, which was later suggested to be caused by internal gravity waves by Aerts & Rogers (2015) and Bowman et al. (2019b). The complex pulsations in rapidly rotating Be stars also became accessible with *CoRoT* (Neiner et al. 2009; Diago et al. 2009; Gutiérrez-Soto et al. 2009; Neiner et al. 2012), similarly demonstrating that more theoretical work is needed, in understanding the diverse variability observed in early-type stars.

Here, we focus on the detection of new heat-driven OB-type variable stars, which are stars whose oscillations are driven by the κ-mechanism (Kiriakidis, El Eid & Glatzel 1992; Moskalik & Dziembowski 1992; Gautschy & Saio 1993; Dziembowski & Pamiatnykh 1993; Dziembowski, Moskalik & Pamyatnykh 1993), discovered in the *K2* space mission data. There are two main types of pulsator amongst early-type stars: SPB stars (Waelkens 1991), which have an approximate range of log $T_{\rm eff} \in [4.05, 4.35]$ and log $L/L_\odot \in [2.0, 4.0]$, and the hotter, more massive β Cep pulsators (Frost 1902, and see the overview given by Stankov & Handler 2005) which have an approximate range of log $T_{\rm eff} \in [4.25, 4.50]$ and log $L/L_\odot \in [3.2, 5.0]$.

Although the oscillations are driven by the same mechanism, the character of the pulsations is different: high-order g modes are typically found in SPB stars, and low-order p and g modes in β Cep stars. The particular opacity bumps responsible for mode excitation in OB-type stars have been found to be the partial ionization layers of iron-group metals (Dziembowski & Pamiatnykh 1993; Dziembowski et al. 1993; Pamyatnykh 1999). There are many factors influencing the driving zones, such as the chemical composition, atomic diffusion, macroscopic mixing, and stellar metallicity. Attempts at defining instability regions are in general agreement — Pamyatnykh (1999) presented a discussion on the instability region of the κ-mechanism in the upper main sequence. Deng & Xiong (2001) argued that core overshoot has little effect on the iron bump opacity shape, based on linear stability analyses of stellar models. Moravveji (2016) investigated the effects of enhancing the iron and nickel opacities in early-type stars and found the instability regions were wider. More recently, Szewczuk & Daszyńska-Daszkiewicz (2017) studied the effect of rotation on the instability region. One of their results is that rotation has a major effect on the extent of the instability domains of SPBs in comparison with core overshooting, opacity data, initial metallicity, and initial hydrogen abundance.

The sample of main-sequence massive stars with adequate photometric data for asteroseismic modelling studies remains limited. The *Kepler* field of view (FOV) was purposefully chosen to avoid star-forming regions in which OB-type stars are typically found. Therefore, the number of these stars to study was limited (Balona et al. 2011; McNamara, Jackiewicz & McKeever 2012). *CoRoT* while successful, only provided a handful of stars for which detailed asteroseismic analyses were possible. On the other hand, *K2* (Bowman et al. 2019a), and more recently *TESS* (see Pedersen et al. 2019 for diverse variability of OB stars in *TESS* sectors 1 and 2), have begun to remedy this lack of continuous, long-term, high-precision photometric data for massive stars.

2 METHOD

2.1 The *K2* space mission

In this work, we focus on the data available from the *K2* space mission (Howell et al. 2014), the re-purposed *Kepler* mission. The radiation pressure of the Sun was used to minimize the use of on-board thruster fuel needed for stability. As such, an individual portion of the ecliptic was monitored for up to 90 d, until it was necessary to rotate the spacecraft to prevent the Sun from entering the telescope's FOV. Each of these monitoring campaigns viewed a new field, allowing for the measurement of objects that were not visible in the original *Kepler* field. Of particular interest for massive star research were Campaigns 2, 9, and 11 as these included star-forming regions around the galactic bulge, and therefore contained a variety of massive stars. The suitability of *K2* for asteroseismology of OB-type stars has been demonstrated in the past, including studies for O stars in Campaign 0 (Buysschaert et al. 2015), chemically peculiar and magnetic stars (Buysschaert et al. 2018a; Bowman et al. 2018), evolved early-type stars (Aerts et al. 2018b), and B-type stars (Balona 2016; White et al. 2017; Aerts et al. 2018b).

2.2 Light-curve extraction

Target pixel data for targets observed by *K2* can be retrieved from MAST.[1] *K2* data contain systemics due to the pointing jitter of the spacecraft (Vanderburg & Johnson 2014; Aigrain, Parviainen & Pope 2016). Thruster firings occurred every ∼6 h to correct the satellite pointing. To extract the photometry from the target pixel frames we follow the methodology of Buysschaert et al. (2015, 2018a). An optimal pixel mask is defined semi-automatically, including all pixels containing flux from the target by means of

[1] Mikulski Archive for Space Telescopes (MAST), https://archive.stsci.edu/

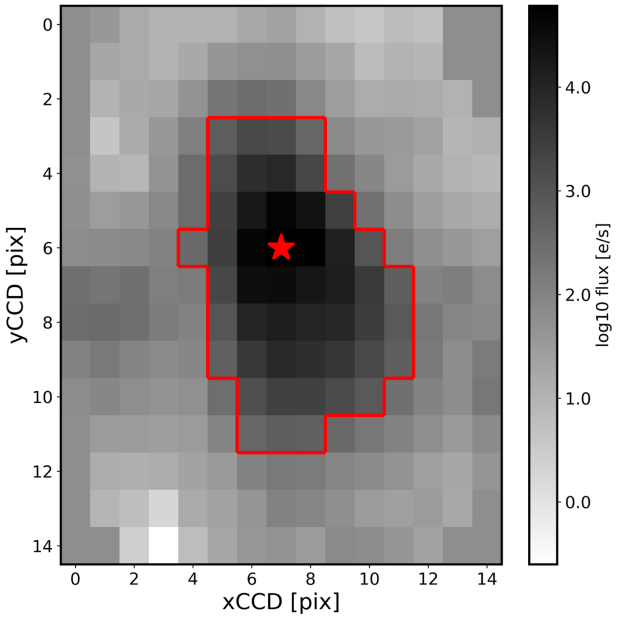

Figure 1. Example of a pixel mask for EPIC 202929357. The abscissa and ordinate indicate the CCD X and Y pixel location. The grey-scale bar shows the total flux. The red contour indicates the definition of the mask. The central star symbol is the centroid of the star and is where the semirandom walk is initiated.

a semirandom walk whilst carefully avoiding possible sources of contamination from nearby or background stars. An example of such a mask is given in Fig. 1, for the newly discovered β Cep star EPIC 202929357. The flux counts within the optimum mask are summed at a given time stamp to produce a light curve.

We subsequently applied the K2SC software package (Aigrain et al. 2016). This pipeline uses Gaussian Process regression to model both position (pointing systematics) and temporal (intrinsic to the star and any other non-positional systematics) variability simultaneously. White noise is handled as a third component. Gaussian Process regression is well suited for this purpose as it does not require any prior information of the stellar variability, see Aigrain et al. (2016) and references therein. After applying K2SC, persisting long-term trends – if present – were removed by fitting a low-degree polynomial. These may be physical but information regarding these trends is unprocurable in the limited *K2* time base.

Generally the time span of each campaign is between 70 and 80 d. The frequency resolution of the extracted data is therefore $1/80 \approx 0.01$ d^{-1} in the best case, which provides us with an upper limit on the frequency uncertainty when extracting independent pulsation mode frequencies from pre-whitening (Aerts et al. 2010). *K2* Campaign 0 has two large gaps in the first 40 d, and generally only the last 30 d are usable. This results in a decrease in frequency resolution $1/30 \approx 0.03$ d^{-1}. For stars in Campaigns 9 and 11, where five of the eight of the stars in this study originate, a significant gap of $\sim$3 d occurs at BJD 24572694 in Campaign 9 and at BJD 24572847 in Campaign 11. This reduces the duty cycle. The different parts were extracted and detrended separately. For the frequency analysis, they were stitched together again. All light curves are measured in long cadence at 29.5 min, resulting in a Nyquist frequency of $\nu_{\rm Ny} \approx 24.47$ d^{-1}.

2.3 Star sample

To find new β Cep stars with *K2*, our sample comprises stars from *Guest Observer Proposals* for massive star asteroseismology. The proposed targets were chosen based on their spectral types being either O or B in SIMBAD, and included stars in different stages of evolution. To separate the targets we viewed the periodograms of the reduced light curves and scanned for signs of coherent modes visually. We filtered our sample, a total of 130 OB-type stars, for stars which show multiperiodic variability consistent with coherent pulsation modes, and excluded potential binaries as it is difficult to ascertain from which star the pulsations originate. The selected list of eight OB variables with dominant variability in the high-frequency regime observed by *K2* is given in Table 1.

2.4 Frequency analysis

We perform *iterative pre-whitening* as developed by Degroote et al. (2009) and improved by Pápics et al. (2012) of the *K2* light curves of stars in Table 1. At each step of the iterative pre-whitening, we calculate the Lomb–Scargle (LS, Lomb 1976; Scargle 1982) periodogram of the light curve, followed by an identification of the frequency with the highest amplitude. This frequency value, along with previous frequencies, are used to perform a non-linear least-squares fit to the light curve using

$$x_{\rm i}(t_{\rm i}) = \sum_{j} A_{\rm j} \sin\{2\pi[\nu_{\rm j}(t_{\rm i} - t_0) + \phi_{\rm j}]\} + C, \quad (1)$$

where $A_{\rm j}$ and $\phi_{\rm j}$ are the amplitude and phase, $\nu_{\rm j}$ the frequency, and t_0 is the zero-point of a star's light chosen as the first observation. Here, $j = 1, ..., n$ is the unknown number of pulsation frequencies and $i = 1, ..., N$ with N the number of data points in the observed light curve. After each iteration, the new multifrequency model is then subtracted from the light curve, and a new iteration commences using the residuals. This scheme is repeated until the signal-to-noise ratio (S/N) of a peak in the LS periodogram, calculated in an interval of width 1 d^{-1} centred around the frequency, is below five following Baran, Koen & Pokrzywka (2015). This criterion is based on simulations of the 90 d time base typical of *K2*. Using this conservative criterion of S/N $\geq$5 coupled over a narrow-frequency range where the dominant variability occurs, allows us to avoid overinterpretation of the data for a typical light curve in the sample, and prevents the introduction of spurious frequencies into the frequency list.

An important limitation for data sets of this time span is the frequency resolution, and careful consideration of the pre-whitened frequencies is recommended. Loumos & Deeming (1978) determined that two frequencies cannot be distinguished when their difference is less than 1.5 times the frequency resolution. We followed this criterion, i.e. when two significant frequencies are closer to each other than 1.5 times the resolution, the lowest amplitude peak is eliminated from the final frequency list. Combination frequencies of the form $n\nu_{\rm i} + m\nu_{\rm j}$, with $n, m \in \mathbb{Z}$, may also be in the frequency spectra and have been detected for β Cep stars (Handler et al. 2004, 2006; Degroote et al. 2009). To search for combination frequencies, we identify base frequencies as the dominant frequencies and scan for combinations of different orders with $n, m \in [-3, 3]$ in a semi-automatic way. We use the frequency resolution ($1/\Delta T$) as the matching criterion, and therefore list the values for each of the data sets. It has been shown by Pápics (2012) – using simulated data and real examples – that as the order of the combination increases, the number of frequencies identified as a combination increases and

Table 1. Sample of OB stars in *K2* fields showing independent coherent pulsations in the high-frequency regime. References are made to the spectral type classification or to previous photometric studies of the object.

Campaign number	EPIC ID	Star name	RA	Dec.	V_{mag}	Spectral type	ΔT (d)	N_{obs}	References
0	202060092	HD 256035	06 22 58.24	+ 22 51 46.17	9.21	O9V:p	36.19	1679	1,2,3
2	202691120	CD-28 12286	16 41 01.98	−28 43 20.86	10.32	OB$^-$	76.94	1904	4
	202929357	CD-27 10876	16 16 15.05	−27 51 19.91	10.95	OB$^-$	64.25	2302	4
9	223832867	HD 164741	18 03 44.08	−25 18 45.08	9.19	B2Ib/II	71.34	3055	5,6,7
	227552090	HD 169173	18 24 08.16	−17 51 48.73	9.93	B3Ib	71.34	2964	5,6
11	233986359	HD 156491	17 18 38.77	−21 35 21.81	9.54	B3III	71.59	2957	5
	235094159	LS 3978	17 13 01.32	-24 12 18.88	12.68	B2III	72.51	3012	8
	235151005	HD 157548	17 24 51.63	−23 55 33.94	8.8	B5III	72.08	2971	5

Notes: References: (1) Negueruela, Steele & Bernabeu (2004), (2) Buysschaert et al. (2015), (3) Balona (2016), (4) Drilling & Bergeron (1995), (5) Houk & Smith-Moore (1988), (6) Pigulski & Pojmański (2008), (7) Hohle, Neuhäuser & Schutz (2010), and (8) Vijapurkar & Drilling (1993).

Table 2. Frequency list for EPIC 202060092 extracted by pre-whitening. The term between brackets in the ID column denotes which group the particular frequency belongs to. The standard deviation of the residuals is 0.068 mmag.

ID	Frequency (d^{-1})	Amplitude (mmag)	SN	Notes
ν_1 (fg2)	3.424(2)	1.9(2)	9.8	
ν_2 (fg2)	3.667(2)	1.3(2)	8.4	
ν_3	6.985(2)	1.2(2)	18.2	$\nu_2+\nu_5$, $2\nu_9$, $4\nu_6$
ν_4 (fg1)	1.674(2)	1.2(2)	5.8	
ν_5 (fg2)	3.319(3)	1.0(2)	6.2	$2\nu_4$
ν_6 (fg1)	1.745(3)	1.0(2)	6.0	
ν_7 (fg2)	3.563(3)	0.9(2)	6.5	
ν_8 (fg1)	1.599(3)	0.7(1)	5.0	
ν_9 (fg2)	3.489(3)	0.7(1)	5.4	

one should be careful not to misinterpret physical frequencies as combinations due to either a low-frequency resolution or to high-order combinations.

By scanning for linear combination frequencies we are identifying mathematical combinations, irrespective of their origin. Due to the limited frequency resolution of *K2* data we cannot infer a physical interpretation. If we list a frequency as a combination, it means that we identify it to be a mathematical match within the frequency resolution of the light curve. For a general discussion on the various physical origins of combination frequencies, we refer to chapter 6 of Bowman (2017).

3 RESULTS

In this section, we present the results of the frequency extraction as described Section 2.4, in the form of light curves, periodograms, and frequency lists. The errors on the frequencies and amplitudes are computed from the non-linear least-squares fitting described in Section 2.4. To correct for the correlated nature of oversampled data, we use the correction factor as defined by Schwarzenberg-Czerny (2003), and calculated following Degroote et al. (2009) and Pápics et al. (2012). The frequency list of the β Cep star EPIC 202060092 is given in Table 2, with the remaining frequency lists are given in Appendix A. The errors on the frequencies and the amplitudes are given as the last digit, written in brackets after each value. The last column in each table indicates if it has been identified as a combination or a harmonic. In the caption of each table, we include the standard deviation of the residuals, at the point where the next frequency drops below S/N = 5 in a 1 d^{-1} window, as an indication of the noise level.

3.1 EPIC 202060092 – HD 256035

In a spectroscopic study by Negueruela et al. (2004), EPIC 202060092 was classified as O9V:p and it was suggested to be a spectroscopic binary because of its broad Hα and HeI 6678 lines. The star was included in the sample of Buysschaert et al. (2015) in which it was confirmed to be a spectroscopic binary with at least one star in the system thought to be a β Cep star based on the frequency spectrum. The dominant frequency is found to be $\nu = 3.424(5)$ d^{-1} and other mode frequencies occur in the range $0.11 \leq \nu \leq 6.99$ d^{-1}.

Because of the two major gaps in the first 40 d of the *K2* photometry, only the data points after 1936.0 (BJD−2454833.0) were extracted and run through *k2sc*. This yielded a total of 36.19 d and 1679 data points resulting in a duty cycle of ∼97 per cent. The frequency resolution is 0.028 d^{-1}. The detrended light curve is given in the top panel of Fig. 2 and the LS periodogram is shown in the bottom panel. Dashed lines indicate independent frequencies, and dotted lines identify combination frequencies.

Iterative pre-whitening reveals nine significant frequencies with amplitudes ranging between 0.6(1) and 1.9(2) mmag which is the lowest dominant peak in our sample. Frequency groups are seen between $1.5 \leq \nu \leq 2$ d^{-1} (labelled as frequency group 1, fg1), and between $3 \leq \nu \leq 4$ d^{-1} (labelled as frequency group 2, fg2). Some frequencies in one group can be found as combinations of the other group, and vice versa, as was already noted by Buysschaert et al. (2015, see their fig. 1 and table 2). Due to the poor frequency resolution, we cannot determine whether these combinations are real or coincidental. This phenomenon is a general feature of the analysed stars and is due to the limited time span of the *K2* data.

Despite the additional detrending with K2SC, the light curve does not yield more identified frequencies than found by Buysschaert et al. (2015); our list consists of nine. It can be seen from the red curve in the bottom panel of Fig. 2 that variability is still present in the residuals. However, pre-whitening beyond our stop criterion leads to unresolved frequencies and is therefore omitted. It should also be noted that the frequency lists do not match with Buysschaert et al. (2015), they identify additional low frequencies < 1 d^{-1} (as harmonics) and one at 1.32(1) d^{-1}. Frequency $\nu_8 = 1.599(3)$ d^{-1} in our list is not detected by them. The differences can largely be explained by the extraction and detrending procedure; Buysschaert et al. (2015) did not use K2SC. This highlights the importance and impact of detrending on extracted pulsation modes in variable stars

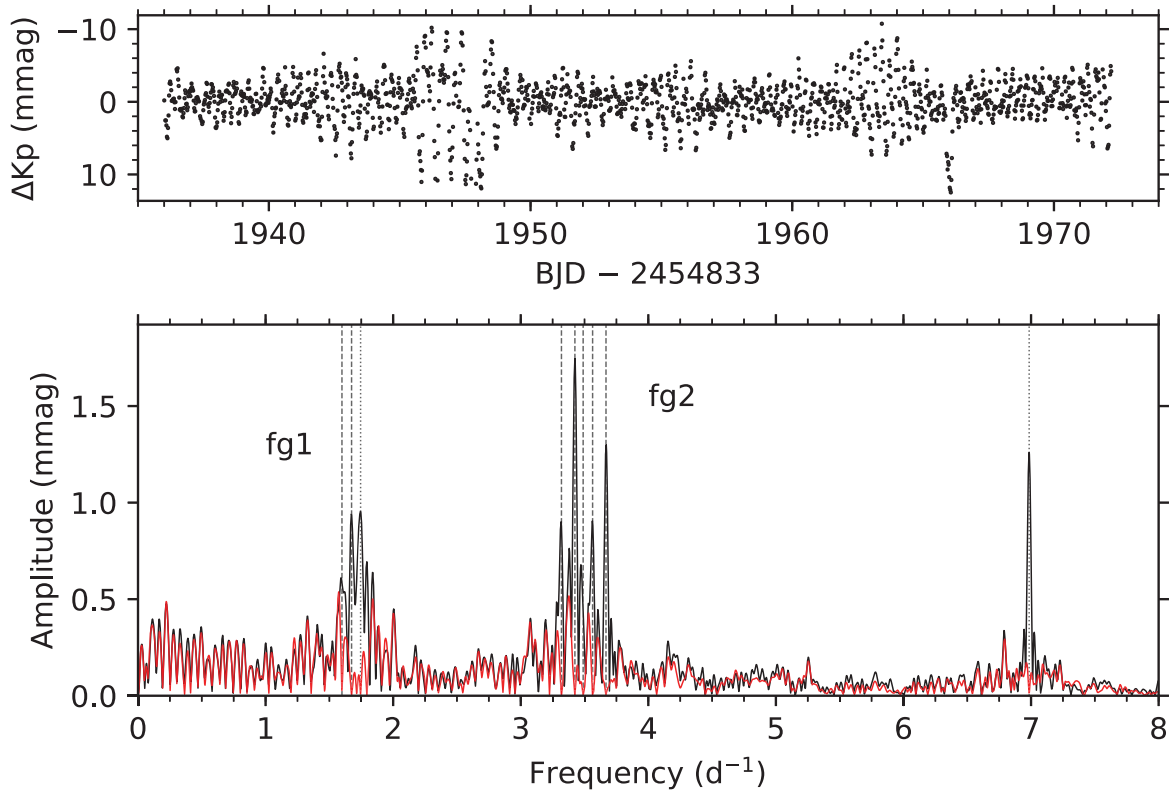

Figure 2. Top: *K2* light curve of EPIC 202060092 with the brightness variations in mmag. Bottom: LS periodograms and frequencies identified by pre-whitening. The initial periodogram is shown in black, while the periodogram of the residuals after pre-whitening is given in red. Dashed lines correspond to independent frequencies, the dotted lines represent low-order combinations/harmonics.

and any subsequent frequency analysis. Clearly, data covering a longer time span are needed to fully resolve and characterize the frequency groups, and confirm EPIC 202060092 as a g- or p-mode-dominated star.

3.2 EPIC 202691120 – CD-28 12286

This star was observed by *K2* in Campaign 2 and classified by Drilling & Bergeron (1995) as OB$^-$ in their galactic OB survey. Stars that showed nearly continuous spectra were assigned spectral OB, with OB$^+$, OB, OB$^-$ indicating increasing Balmer absorption-line strength. This is based on the original photographic plate classification scheme by Nassau & Stephenson (1960), who segregated OB stars based on hydrogen-line strength and used this to classify any star earlier than B6. The authors do note that late B-type and early A-type supergiants may be misclassified as OB, as their hydrogen line imitates that of the OB stars. The presence of the Ca II line is used to segregate the A stars, such that main sequence A stars are unlikely to be classified as OB. A total of 1904 *K2* data points were extracted, over 76.94 d, which implies a duty cycle of only ∼51 per cent. This is a result of a large number of poor quality flags near the end of the time-series, resulting in their removal by the K2SC module. The detrended light curve is given in the upper panel of Fig. 3. The LS periodogram, shown in the bottom panel of the same figure, indicates frequencies between 0 and 10 d^{-1}.

A total of 13 frequencies were extracted by the pre-whitening, which have amplitudes between 0.7(1) and 8.3(3) mmag. Two of the lower frequencies are combinations, leaving five independent ones below 2 d^{-1} and six above 6 d^{-1}. Therefore, we interpret the independent low frequencies as low amplitude g modes. The higher frequencies are coherent oscillations. If we take the differences between successive frequencies in the high-frequency regime we retrieve three splittings of ∼0.44 d^{-1}, two between the three highest frequencies up to ν_1 and one between ν_2 and a lower amplitude frequency. In addition, two splittings of ∼0.60 d^{-1} become apparent, one next to ν_2 and one between two lower amplitude frequencies. These equidistant frequencies might be due to rotational splitting. Of course we cannot unambiguously claim that these frequencies belong to the same multiplets, see for example, the identification of a previously claimed multiplet to three different modes in the β Cep star 12 Lacertae (Handler et al. 2006). Other methods such as multipassband photometry are needed to confidently assign the geometries of these modes. The frequency list is given in Table A1, demonstrating that EPIC 202691120 is predominantly a p-mode pulsator. The presence of low frequencies that cannot be identified as combination frequencies of the p modes makes us classify the star as a hybrid β Cep/SPB.

3.3 EPIC 202929357 – CD-27 10876

This star was classified by Drilling & Bergeron (1995) as having a spectral type of OB$^-$. The *K2* Campaign 2 light curve and LS periodogram are shown in Fig. 4, in the upper and bottom panels, respectively. The detrended light curve contains 2302 data points over 64.25 d. This yielded a duty cycle of ∼75 per cent. The frequency resolution is 0.015 d^{-1}.

Pre-whitening leads to a total of 23 frequencies. Nearly all the frequencies detected in EPIC 202929357 are detected in the high-

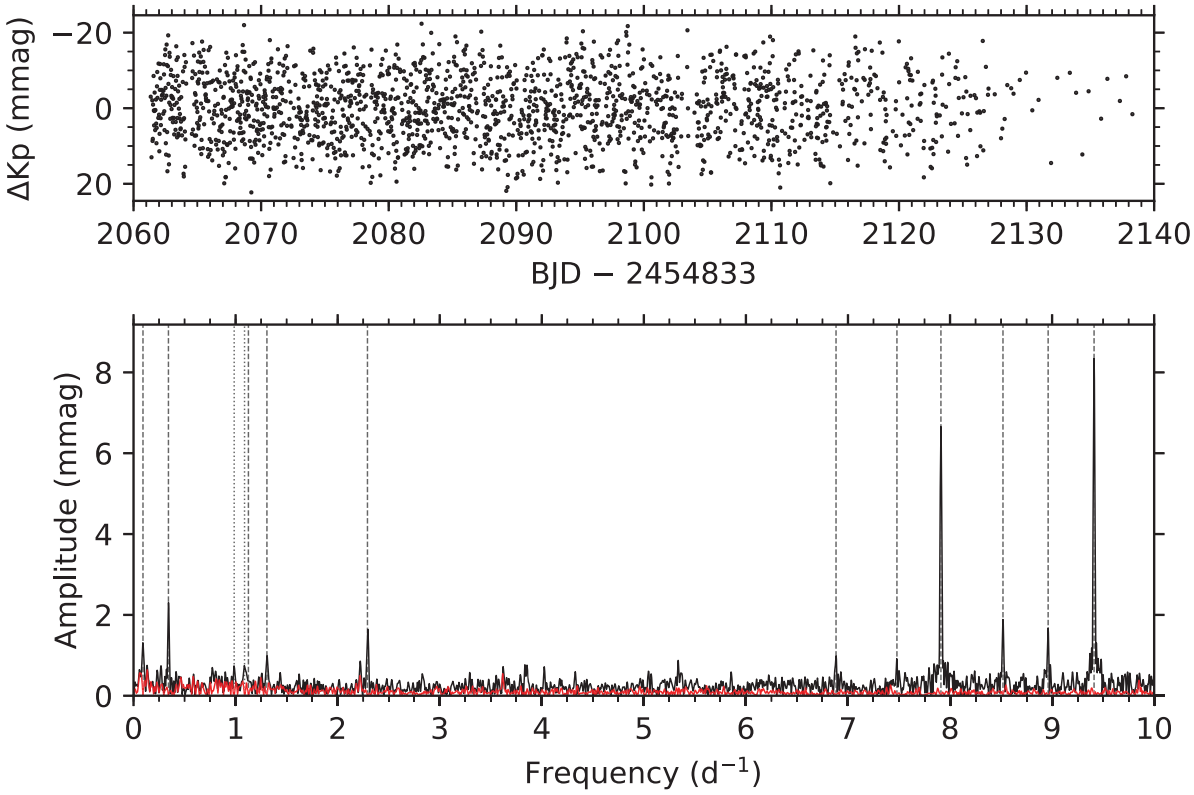

Figure 3. Top: *K2* light curve of EPIC 202691120 with the brightness variations in mmag. Bottom*:* LS periodograms and frequencies identified by pre-whitening. The linestyles are the same as in Fig. 2. No significant frequencies beyond 10 d^{-1} are detected.

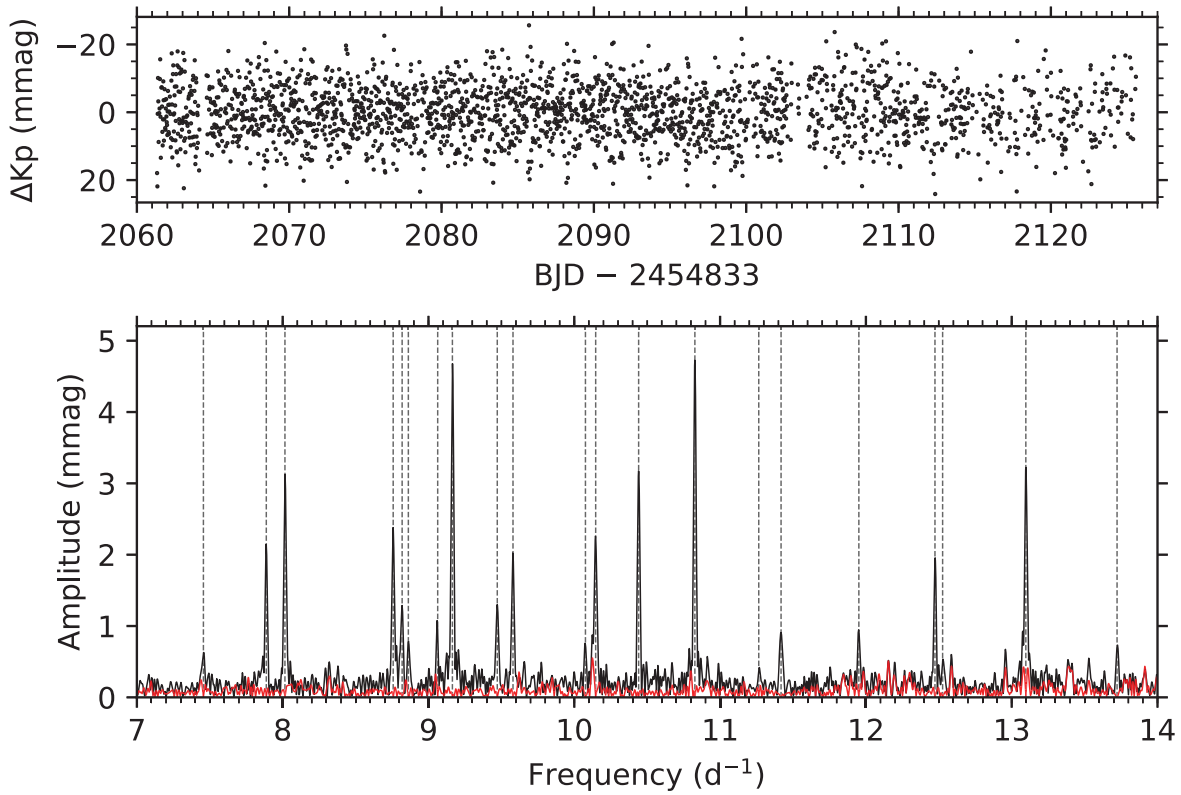

Figure 4. Top: *K2* light curve of the newly discovered β Cep star EPIC 202929357 with the brightness variations in mmag. Bottom: LS periodograms and frequencies identified by pre-whitening. The linestyles are the same as in Fig. 2.

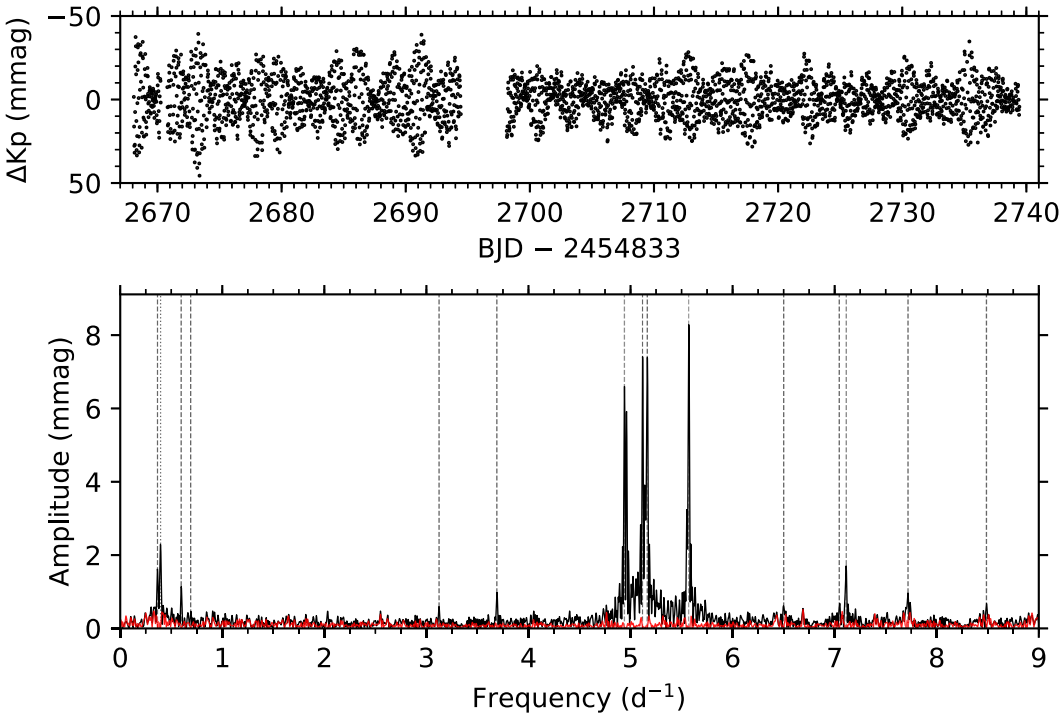

Figure 5. Top: *K2* light curve of EPIC 223832867 with the brightness variations in mmag. Bottom: LS periodograms and frequencies identified by pre-whitening. The linestyles are the same as in Fig. 2.

frequency regime > 7 d^{-1}. Only two lower frequencies, $\nu_{15} = 4.0458(9)$ d^{-1} and $\nu_{16} = 0.051(1)$ d^{-1} are identified. The amplitudes range between 0.6(1) and 4.7(2) mmag. In the periodogram in Fig. 4, we only show the high-frequency region for good visibility. No low-order combinations are detected so we infer that all identified frequencies are due to independent modes. The frequencies were scanned for similar spacings in order to detect possible rotational splitting, but none could be identified unambiguously.

Similarly to EPIC 202691120, EPIC 202929357 has high-frequency p modes indicative of a young massive β Cep star. Moreover, only two frequencies are detected below 5 d^{-1} such that the star is predominantly a p-mode pulsator. A longer time-series, high-resolution spectroscopy, or multicolour photometry, might aid in mode identification. None the less, the coherent character of the high-frequency modes, together with the spectral type OB, allows us to classify this star as a new β Cep variable.

Despite the rough OB classification and lack of spectroscopy, we do need to address whether the presence of p-mode pulsations is enough to classify the Campaign 2 stars EPIC 202691120 and EPIC 202929357 as β Cep. Lower mass stars (A2 – F2), in the δ Scuti instability region show variability on similar time-scales (Rodríguez & Breger 2001) and SIMBAD gives estimates between 7500 and 9300 K for EPIC 202691120 and EPIC 202929357. However, these values are from Huber et al. (2016), who use synthetic star populations sampled from distributions lacking massive and pre-main-sequence stars. The authors encourage users of the EPIC catalogue (Ecliptic Plane Input Catalog) to use other observational information instead – such as colours – to preliminary characterize these types of stars (Huber et al. 2016) in the absence of derived spectroscopic parameters. We therefore verify the β Cep classification by using *Gaia*-DR2 (second data release) photometry and by placing the stars in a colour–magnitude diagram (CMD), see Section 4, confirming the SIMBAD classification as OB.

3.4 EPIC 223832867 – HD 164741

The object is classified as a B2Ib/II star (Houk & Smith-Moore 1988) and was identified as a β Cep by Pigulski & Pojmański (2008) with a dominant frequency of 5.119632(19) d^{-1}. They report four additional independent modes, with a detection threshold of 3.9 mmag, using 474 ground-based observations covering 2847 d. EPIC 223832867 was also studied by Hohle et al. (2010), who calculated the masses and luminosities of OB stars detected in the 2MASS (Two Micron All-Sky Survey) and *Hipparcos* surveys using multicolour photometry, spectral types, extinctions and revised *Hipparcos* distances. The estimated mass of EPIC 223832867, 6.3 ± 0.4 M$_\odot$, is typically lower than expected for β Cep pulsators but many factors can influence the exact boundaries of the theoretical β Cep instability region (see Miglio, Montalbán & Dupret 2007). The bolometric luminosity and the effective temperature have also been estimated to be $\log(L/L_\odot) = 3.12 \pm 0.03$ and $\log T_{\rm eff} = 4.28^{+0.04}_{-0.05}$ K. The star is classified as a Be star (Jaschek & Egret 1982; Steele, Negueruela & Clark 1999; Barnsley & Steele 2013), based on the Hα emission. The projected rotational velocity of the object was determined to be $v \sin i = 77$ km s^{-1} (Steele et al. 1999), which is moderate so it is likely seen at low inclination.

Stitching the two sub-campaign *K2* light curves of EPIC 223832867 yields 3055 data points over 71.34 d, resulting in a duty cycle of ∼89 per cent. The frequency resolution is 0.014 d^{-1}. The light curve is shown in the upper panel of Fig. 5 and shows both short-term variations and a long-term beating pattern. An amplitude difference between the sub-campaigns is noticeable. We do not observe this in the other Campaign 9 star, EPIC 227552090 (Fig. 6), and therefore argue that it is unlikely instrumental. The LS periodogram in the bottom panel of Fig. 5 shows low ($\leq$1 d^{-1}) and high ($4 \leq \nu \leq 8$ d^{-1}) frequencies. A total of 15 are identified from pre-whitening. The amplitudes range between 0.5(1) and

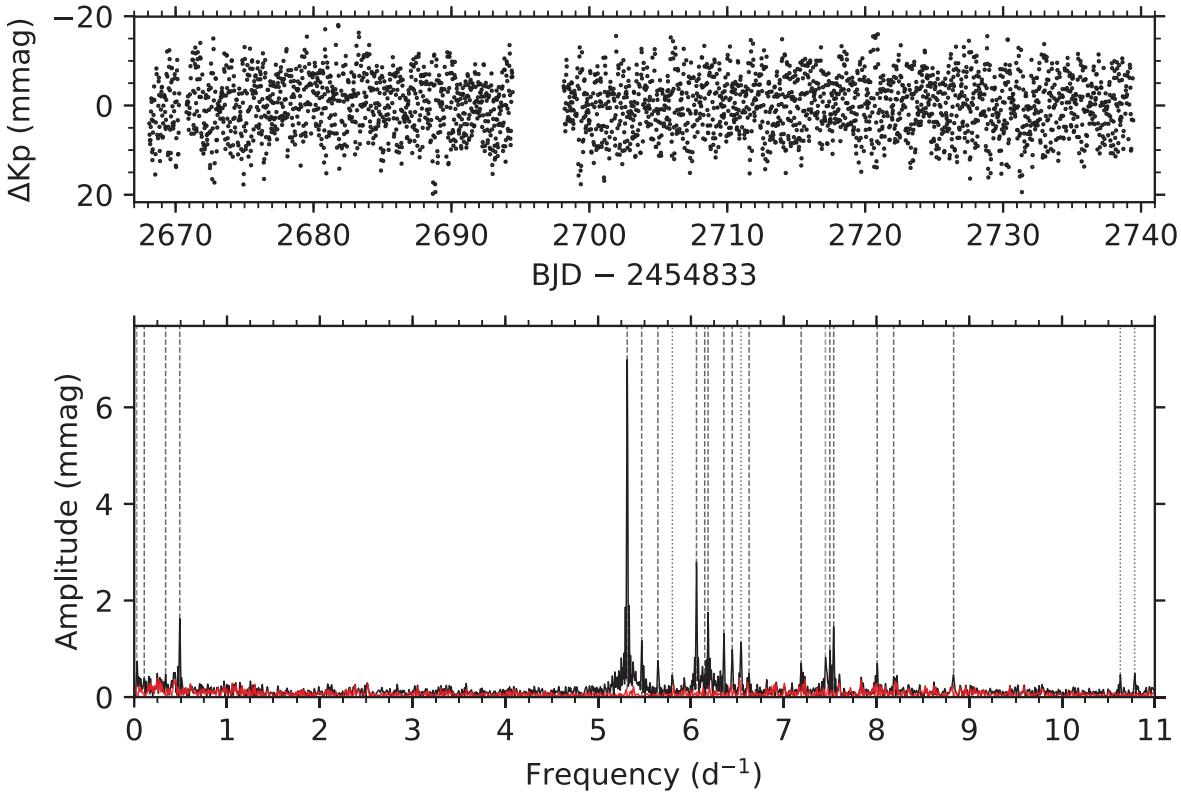

Figure 6. Top: *K2* light curve of EPIC 227552090 with the brightness variations in mmag. Bottom: LS periodograms and frequencies identified by pre-whitening. The linestyles are the same as in Fig. 2.

8.4(5) mmag. The first four high-amplitude frequencies all appear as a doublet structure in the periodogram. The close proximity of the frequencies in these doublets leads to the Loumos & Deeming (1978) criterion being satisfied ($<1.5/\Delta T$, with ΔT the time base of the light curve) for three of the eight members. We do not consider them in the frequency list as they are formally unresolved from each other given this criterion, although they are likely real. Only one doublet is sufficiently separated to be kept as two frequencies in the frequency list. The light curve in Fig. 5 exhibits beating patterns that are likely caused by unresolved close-frequency pulsations at both high and low frequency (see e.g. Bowman et al. 2016), combined with rotation. The low-frequency peak with the highest amplitude is identified as the combination frequency, $\nu_5 \approx \nu_1 - \nu_2 = 0.3949(6)$ d^{-1}.

Further data, spanning a longer time span are necessary to fully characterize the beating patterns produced by the close-frequency pulsation modes in EPIC 223832867. The frequency list is given in Table A3 and is consistent with the earlier results by Pigulski & Pojmański (2008). We denote the frequencies identified by them in the last column in Table A3.

3.5 EPIC 227552090 – HD 169173

The star has spectral type B3Ib (Houk & Smith-Moore 1988). Pigulski & Pojmański (2008) identified this star as a β Cep star, finding only one frequency ($\nu_1 = 5.31303(3)$ d^{-1}) using 789 data points of ASAS-3 (All-Sky Automated Survey) photometry.

The *K2* light curve EPIC 227552090 is given in the upper panel of Fig. 6 and consists of 2964 data points over 71.34 d. The duty cycle is therefore ∼86 per cent and the frequency resolution is 0.014 d^{-1}. The LS periodogram, shown in the lower panel of Fig. 6, reveals a dominant frequency of $\nu_1 = 5.3131(2)$ d^{-1} confirming the result by Pigulski & Pojmański (2008). We detect a total of 24 frequencies with amplitudes ranging between 0.39(8) and 7.0(2) mmag, of which three have been identified as possible combination frequencies. We identify two separate frequency series, visible in Fig. 7. The first series is marked by the green dashed–dotted lines and the second by the red dashed lines. The first series starts at $\nu_1 = 5.3131(2)$ d^{-1}, the dominant peak in the LS periodogram, and the second series at the second dominant peak $\nu_2 = 6.0599(4)$ d^{-1}. The spacings are not completely regular, in the first series they average around ∼0.16 d^{-1}. In the second series the spacings range from ∼0.08 to ∼0.09 d^{-1}, all within the frequency errors, if we ignore the first three peaks of the second series in Fig. 7. On the other hand, this second series could very well also be a rotational quintuplet with a missing member, unrelated to the first series.

Furthermore, there is a decrease in amplitude for increasing frequency leading to an asymmetric frequency pattern (see Fig. 7 for a zoom-in of the region where the spacings occur). In each series one member is found as a combination of the highest amplitude peak in that series, that is ν_1 or ν_2, with the highest amplitude peak in the low-frequency regime $\nu_4 = 0.4907(6)$ d^{-1} (i.e. $\nu_{16} = \nu_1 + \nu_4$ and $\nu_7 = \nu_2 + \nu_4$). These are given in the last column of Table A4 and shown as the dotted lines in Fig. 6.

Approximately equally spaced p-mode frequencies have been detected in some massive stars, for example by Degroote et al. (2010) for HD 46149 where spacing of $\Delta\nu = 0.48 \pm 0.02$ d^{-1} was uncovered for short lifetime modes with frequencies between $3.0 < \nu < 7.5$ d^{-1}. Similar oscillations have also been claimed by Belkacem et al. (2009) to occur in V1449 Aql, a star previously

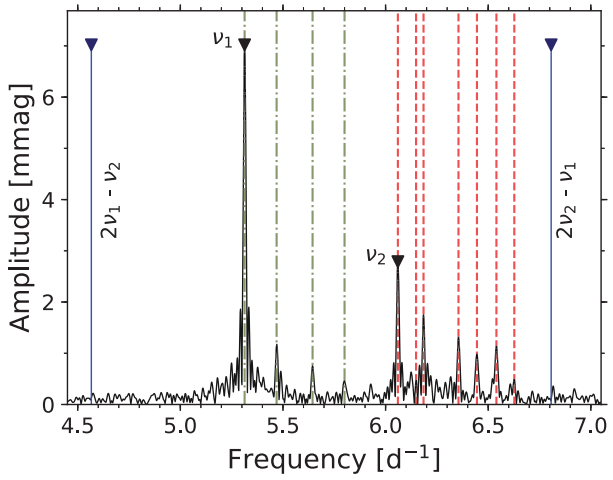

Figure 7. Zoom-in of the region where frequencies equally spaced in frequency are detected in EPIC 227552090. The dashed/dashed–dotted lines are resolved frequencies, and the blue lines depict locations of generated combinations of ν_1 and ν_2 (marked with a black triangle) that are possible within this frequency range. The green dashed–dotted and the red dashed lines indicate frequencies referred to as the first and second series, respectively.

classified as a large amplitude β Cep pulsator. Degroote et al. (2009) proposed non-linear resonant mode excitation as the origin of the frequency spacing pattern instead. They showed that many frequencies in V1449 Aql appear as combinations of the dominant modes and are phase locked ($\phi_z = \phi_x \pm \phi_y$, where x, y indicate the parent frequencies and z the combination), which is not expected for stochastically excited modes. The regular frequency spacing in V1449 Aql was fully reconstructed from combinations of the high-amplitude modes (Degroote et al. 2009).

Also EPIC 227552090 has a dominant mode, twice as large as the next frequency in terms of amplitude. This raises the question whether non-linear resonant mode excitation may also be at work here. Indeed, asymmetric patterns are certainly possible through non-linear resonant mode coupling, as seen in white dwarfs (Buchler, Goupil & Serre 1995). To verify this, we assumed that the two dominant modes in EPIC 227552090, $\nu_1 = 5.3131(2)$ d^{-1} and $\nu_2 = 6.0599(4)$ d^{-1}, are the parent frequencies and generated combinations up to the fifth order. As shown in Fig. 7, none of the generated combination frequencies fall within the frequency resolution of the resolved frequencies. We therefore conclude that non-linear resonant mode excitation is not the origin of the regular frequency spacing in EPIC 227552090.

3.6 EPIC 233986359 – HD 156491

This star is spectral type B3III (Houk & Smith-Moore 1988). It shows emission in Hα (MacConnell 1981) and is therefore classified as a spectroscopic Be star. The *K2* light curve of EPIC 233986359 is shown in the upper panel of Fig. 8. A total of 2957 data points over 71.59 d yields a duty cycle of ∼86 per cent and a frequency resolution of 0.014 d^{-1}. The LS periodogram, shown in the lower panel Fig. 8, reveals the presence of distinct frequency groups labelled as fg0, fg1, and fg2. We extract a total of thirteen frequencies with amplitudes between 1.4(3) and 8.2(5) mmag. The frequency list is presented in Table A5.

The light curve exhibits complex beating patterns caused by the close spacing of frequencies in the two frequency groups, both shown in Fig. 8. The close frequency spacing pattern implies a high local noise estimate. The stop criterion is satisfied rapidly, such that the number of resolved frequencies is limited. We cannot reconstruct all frequencies in one group as combination frequencies from another group. Only the harmonic of the dominant frequency (in terms of amplitude) is found in fg2, $\nu_8 = 2\nu_1$. The low frequencies in fg0 on the other hand can all be explained as differences of the frequencies fg1 suggesting that there may also be independent mode frequencies above 4 d^{-1}. The detected combinations are given in a separate column in Table A5. Fundamental parameters from spectroscopy are needed to model this interesting Be star.

3.7 EPIC 235094159 – LS 3978

This star is of spectral type B2III (Vijapurkar & Drilling 1993). The *K2* light curve is shown in the upper panel of Fig. 9 and consists of 3012 data points over 72.51 d, resulting in a duty cycle of ∼87 per cent and a frequency resolution of 0.014 d^{-1}. The amplitudes of the oscillations are large compared to other stars in our sample. This is advantageous as this is the faintest object (in terms of V magnitude, see Table 1), resulting in a higher noise level than for the other stars. None the less, the LS periodogram shown in the bottom panel of Fig. 9 reveals many independent mode frequencies.

Pre-whitening reveals a total of 35 frequencies with amplitudes between 0.7(1) and 21.3(3) mmag. For visibility, the vertical axis in the bottom panel of Fig. 9 was cut to 10 mmag. We scanned for combinations but no obvious candidates were detected. The frequency with the highest amplitude below 1 d^{-1}, that is $\nu_3 = 0.0381(4)$ i.e. a period of ∼26.25 d, shows multiple harmonics. In fact, many low frequencies <1 d^{-1} can be explained as harmonics of ν_3 up to $9\nu_3$, but $4\nu_3$, $5\nu_3$, $6\nu_3$, and $7\nu_3$ are missing. We cannot identify further frequencies below 4 d^{-1}, besides the harmonic series, as combinations in the high-frequency regime.

The frequency list is given in Table A6. The detected harmonics are indicated in the last column of the same table and suggest that this is a pulsating B star in a binary with ellipsoidal variability or a single B star with rotational modulation, in addition to high-frequency modes. Unfortunately information about the spherical degree ℓ and radial orders n cannot be retrieved so the only current source for seismic input is the frequency list presented here.

3.8 EPIC 235151005 – HD 157548

This star has spectral type B5III according to Houk & Smith-Moore (1988). The *K2* light curve of EPIC 235151005, and its corresponding LS periodogram are shown in Fig. 10. The light curve contains 2971 data points over 72.08 d resulting in a duty cycle of ∼86 per cent and a frequency resolution of 0.014 d^{-1}. A total of 21 significant frequencies are detected, with amplitudes between 0.29(7) and 3.7(2) mmag. In the LS periodogram, we distinguish three distinct groups of low frequencies (<4 d^{-1}), in order of increasing frequency values. This appearance of frequencies in closely spaced groups is similar to EPIC 202060092 and EPIC 233986359. We cannot explain all frequencies in fg1 as combinations of frequencies in fg2, or vice versa.

A category of pulsating stars that show frequencies occurring in distinct groupings are Be-type variables, broadly defined as B-type stars showing emission in Hα. Saio et al. (2007), Neiner et al. (2009), and Balona et al. (2011) noted several instances of frequency groupings in Be stars in a large study of B-type variables observed with the *MOST, CoRoT*, and *Kepler* space missions, respectively. These stars are characterized as fast rotators that may feed mass to circumstellar discs in episodic mass ejections (Porter & Rivinius

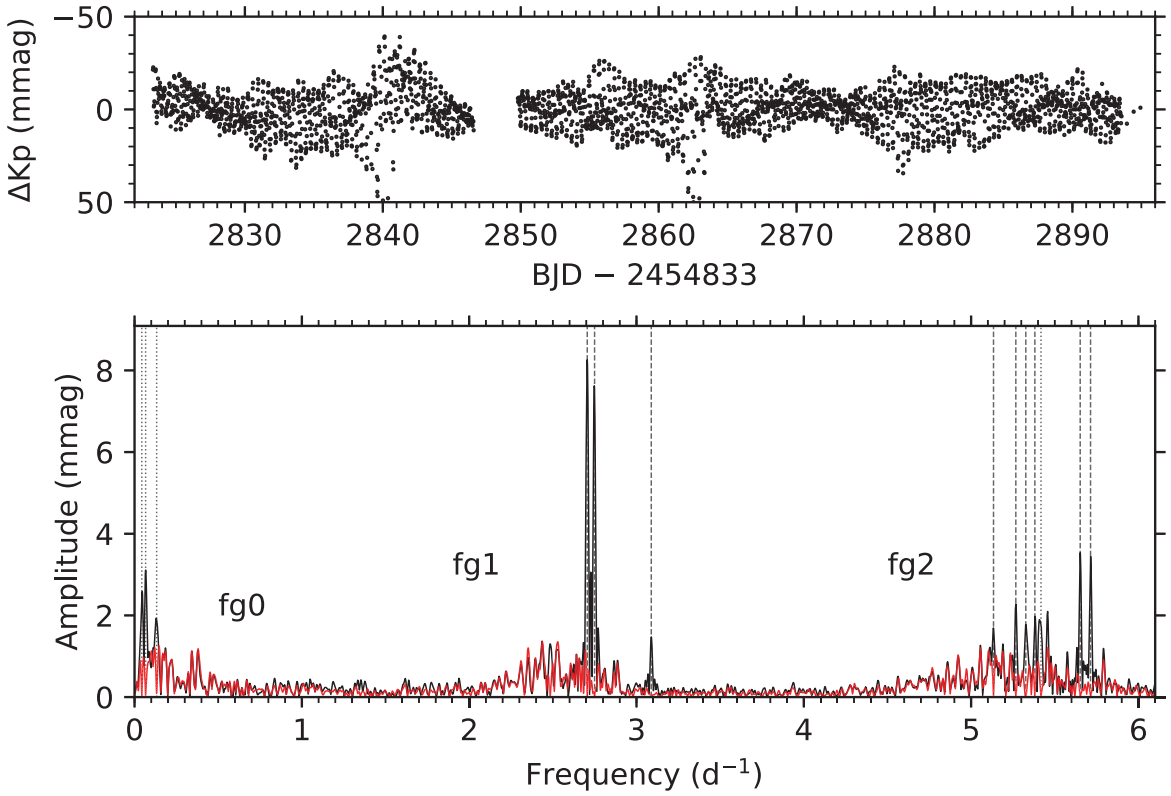

Figure 8. Top: *K2* light curve of EPIC 233986359 with the brightness variations in mmag. Bottom: LS periodograms and frequencies identified by pre-whitening. The linestyles are the same as in Fig. 2.

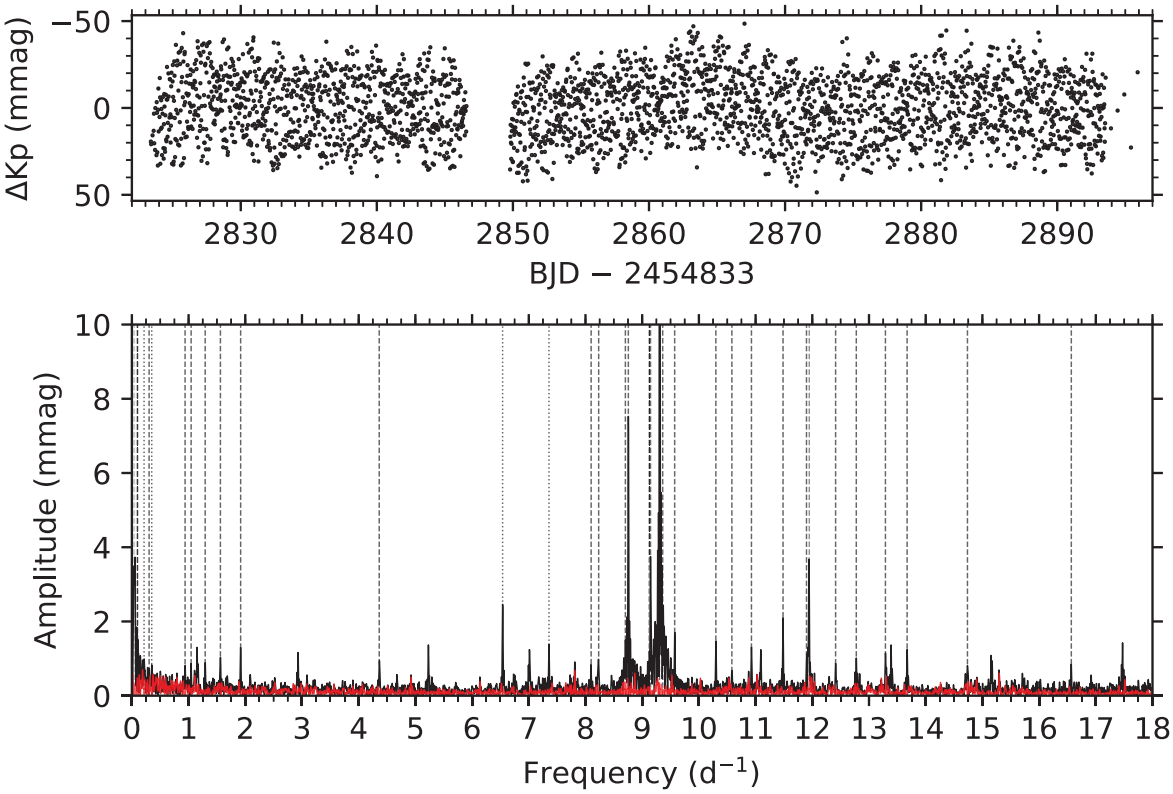

Figure 9. Top: *K2* light curve of EPIC 235094159 with the brightness variations in mmag. Bottom: LS periodograms and frequencies identified by pre-whitening. The amplitude is cut-off at 10 mmag, the dominant peak has an amplitude of 21.3(3) mmag. The linestyles are the same as in Fig. 2.

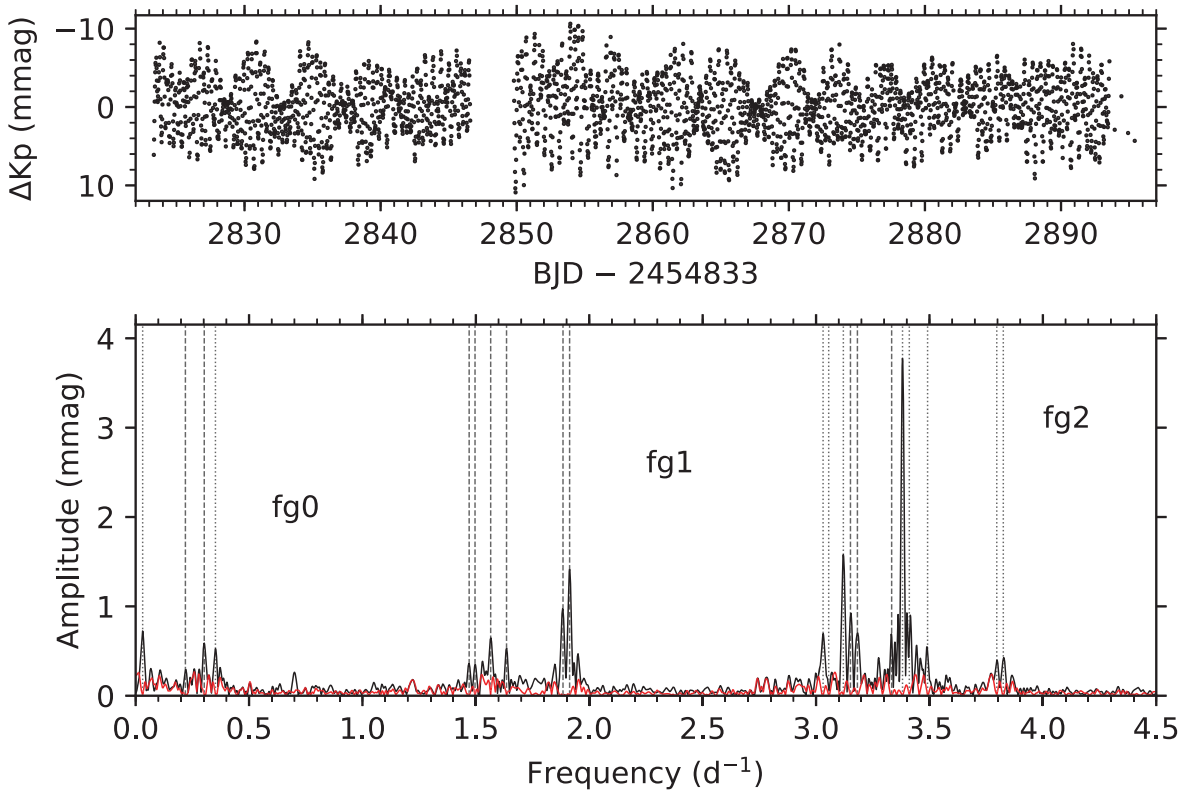

Figure 10. Top: *K2* light curve of EPIC 235151005 with the brightness variations in mmag. Bottom: LS periodograms and frequencies identified by pre-whitening. The linestyles are the same as in Fig. 2.

2003). The irregular outbursts, in the case of HD 49330, have been hypothesized by Huat et al. (2009) as occurring when the close interacting frequencies come into phase with each other. The Be star studied by Kurtz et al. (2015), KIC 11971405, has an amplitude spectrum with striking resemblance to the amplitude spectrum for EPIC 235151005 (Fig. 10). Similar frequency patterns are also seen in the B5IVe star HD 181231 by Neiner et al. (2009), albeit at lower frequencies. In these studies, the authors were able to explain most frequencies in other groups as combinations from a limited set of parent frequencies, identified as g modes.

In the stars showing frequency group structure (EPIC 202060092, EPIC 233986359, and EPIC 235151005), we were not able to interpet all frequencies from a set of parent frequencies. We therefore argue in favour of a hybrid pulsation character as seen in *CoRoT* B2V star HD 170580 (Aerts et al. 2019a) for which the authors similarly were not able to explain all high frequencies as combinations. In this star, also distinct frequency groups were detected, between $1.4 \leq \nu \leq 2\,\mathrm{d}^{-1}$ and $3.1 \leq \nu \leq 3.9\,\mathrm{d}^{-1}$, remarkably similar to what we find for EPIC 235151005. For that very slowly rotating star, the frequencies were identified as modes with radial orders $n \in [-7,2]$. Future spectroscopy will reveal whether these three *K2* pulsators are fast or slow rotators.

4 DISCUSSION

We summarize the discovered variability of the eight *K2* stars in Fig. 11, where we plot an observational CMD using the DR2 of *Gaia* (Gaia Collaboration et al. 2016, 2018). The horizontal axis denotes the difference in the apparent blue and red *Gaia* bandpass brightness in units of magnitude corrected for reddening using values supplied by *Gaia*-DR2 (Andrae et al. 2018). The vertical axis denotes the absolute *G*-band magnitude, corrected for interstellar absorption (Andrae et al. 2018). To construct absolute magnitudes, we use the distance estimations provided by Bailer-Jones et al. (2018). The distances are obtained purely based on geometric properties (i.e. the parallax), independent of any physical properties or extinction values of individual stars. We also include an error bar to indicate the uncertainty related to the average extinction and reddening, based on the *Kepler* targets monitored by *Gaia*.

The size of the circles in Fig. 11 is based on the amplitude of the dominant mode for each star and the colour bar indicates the frequency at which this maximum occurs. In this way, we provide a simple representation of the diverse variability of pulsators in this small sample. As a frame of reference, we included all *Kepler* stars with apparent *G*-band magnitude less than 13.5 mag, and having a *Gaia*-DR2 parallax at least four times above its error (if it is in the data base in the first place). For this, we made use of the gaia-kepler.fun cross-match data base created by Megan Bedell.[2]

All values from *Gaia*-DR2 used for our sample are summarized in Table B1. The location of the rest of the targets on the CMD confirms them as early-type stars, such that the spectral classification from SIMBAD, which we used to select our targets is at least approximately adequate for these stars. For EPIC 233986359, a parallax was not available in *Gaia* DR2, and for EPIC 202929357 no reddening or extinction values were available, so those stars were not included in Fig. 11.

We use the CMD to explore the relative positions and evolutionary stages of the stars in our sample with respect to known B-type

[2]https://gaia-kepler.fun

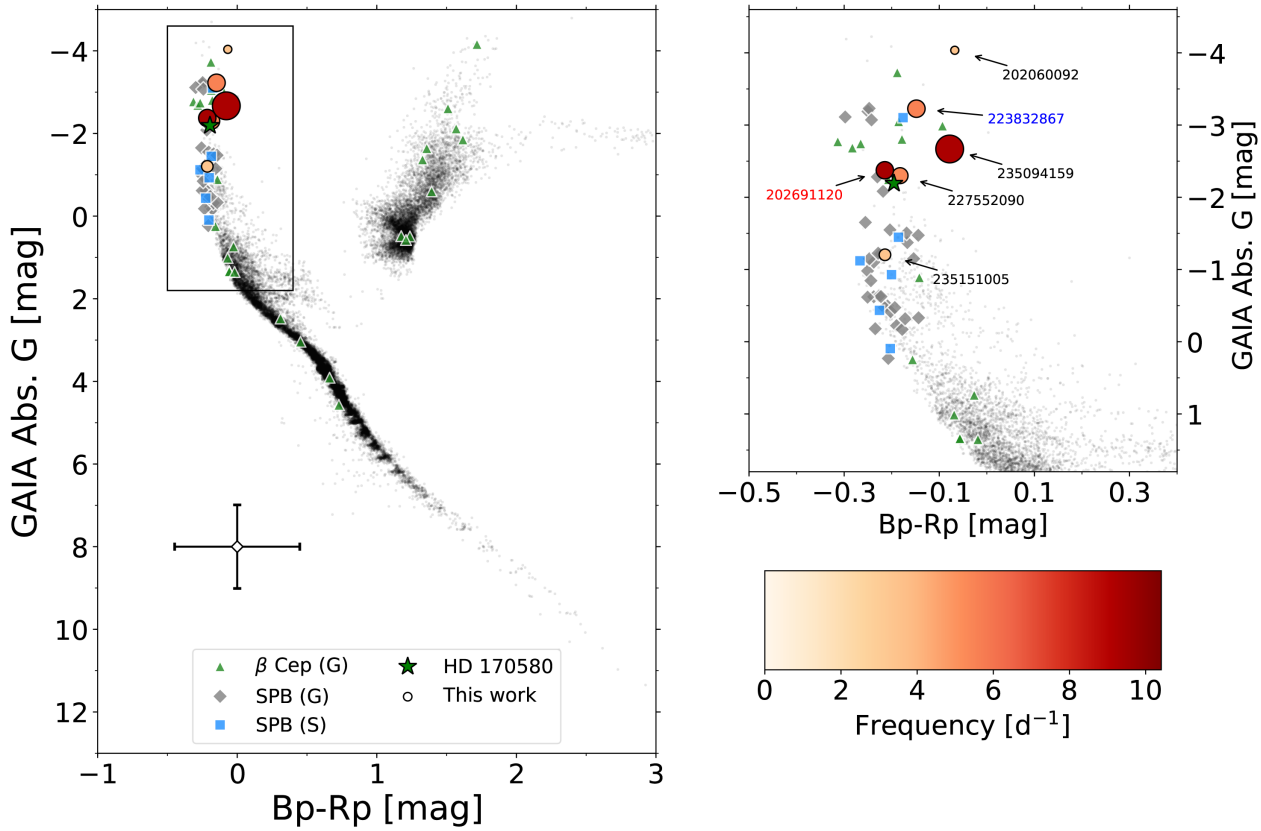

Figure 11. Observational CMD for the targets presented in this work and given in Table 1. The meaning of the symbols is shown in the legend. The size of the circular symbols of the stars in our sample indicates the amplitude of the dominant mode of that star, ranging between 1.9(2) and 21.3(3) mmag, and the colour bar represents the frequency of this mode. The colour of the names indicates if it is observed by *TESS* in two sectors (blue), one sector (red) or not (black). The background points in grey denote all *Kepler* objects for which *Gaia*-DR2 parallaxes are available. We include known β Cep and SPB stars from ground-based photometry (G) and space-age photometry (S) as a frame of reference. The upper right frame shows a zoom of six of the eight newly discovered pulsators in the box marked on the left-hand frame.

pulsators, due to a lack of spectroscopically derived atmospheric parameters $T_{\rm eff}$ and $\log g$. The known B-type pulsators include ground-based (photometry/spectroscopy) discovered SPB and β Cep from lists compiled by P. De Cat as of 2004 January,[3] and space-mission photometry SPB stars as compiled in appendix B in Szewczuk & Daszyńska-Daszkiewicz (2018). One additional star, HD 170580 (Aerts et al. 2019a) is put as a reference for EPIC 235151005. In Appendix B, we verify whether the CMD, in Fig. 11, is a good proxy for the theoretical Hertzsprung–Russell diagram (HRD) in the case where spectroscopic parameters are lacking.

For the *K2* stars in our sample, additional data are needed before seismic modelling is attempted. EPIC 223832867 is visible in *TESS* sectors 3 and 4 consecutively such that a time base of ∼54 d is available. Both EPIC 202691120 and EPIC 202929357 are observed in sector 12, implying ∼27 d of additional photometry. EPIC 202060092, EPIC 233986359, EPIC 235094159, EPIC 227552090, and EPIC 235151005 are unfortunately not observed by *TESS*. These additional *TESS* data will be useful to add to the *K2* photometry. The coherent character of the modes postulates that they have long lifetimes, as expected for β Cep stars. We marked the stars to be observed by *TESS* on Fig. 11 in one sector for ∼ 27 d (red) and in two sectors for ∼ 54 d (blue).

[3] http://www.ster.kuleuven.ac.be/ peter/Bstars/

4.1 The three new β Cep stars

EPIC 202929357 is the richest β Cep in terms of the number of high-amplitude resolved p-mode frequencies. Unfortunately it is not included in the CMD (Fig. 11), but it is similar to EPIC 202691120 with regards to the pulsational character. The location of EPIC 202691120 places it amongst previously known β Cep and confirms the SIMBAD classification. The same spatial location of EPIC 202929357 (the *K2* Campaign 2 FOV) in the ecliptic implies that the reddening is approximately similar in magnitude, which would place it relatively close to EPIC 202691120. Spectroscopy is ultimately needed to confirm the classification formally.

Similarly for EPIC 235094159, the distance to this object is poorly constrained as seen in Table B1, $d = 6000.2^{+2673.3}_{-1548.9}$ pc, leading to an uncertain absolute G magnitude. Moreover, the harmonic series in the low-frequency region points towards a pulsating B star with either ellipsoidal variability or rotational modulation. This has an effect on the observed colours as well. Spectroscopy, to identify the binary system and determine spectroscopic parameters, is needed for unambiguous classification.

4.2 The three stars with frequency groupings

Three stars exhibit structure in the form of frequency groupings: EPIC 202060092, EPIC 233986359, and EPIC 235151005. They cover a wide difference in colours between them (Fig. 11), implying

that the underlying mechanism might not be related. The underlying cause of the structures remains uncertain, as we require additional information in the form of either spectroscopy and/or additional uninterrupted photometry to increase the frequency precision. Not all frequencies can be explained from a set of parent modes.

The incompatibility of explaining the frequency group structure as combination frequencies is similar to the case of HD 170580, which was found to be an evolved star near the Terminal Age Main Sequence (TAMS) (Aerts et al. 2019a). Our results clearly demonstrate the necessity of long-term, continuous, and high-precision photometry for studying the variability of early-type stars. Unfortunately none of the stars exhibiting frequency groupings (EPIC 202060092, EPIC 233986359, and EPIC 235151005) will get observed with the *TESS*.

5 CONCLUSION

The *K2* mission and its changing FOV have allowed us to discover new variables in a sparsely populated blue part of the HRD (Fig. 11). The variable objects include three new β Cep stars (EPIC 202691120, EPIC 202929357, and EPIC 235094159), one known β Cep (EPIC 223832867) for which we present additional low-amplitude frequencies, and three stars exhibiting structure in the form of distinct groups of frequencies (EPIC 202060092, EPIC 233986359, and EPIC 235151005).

Nearly equally spaced frequency patterns were found in EPIC 227552090. Stochastic excitation induced by turbulent motions in the subsurface convection zone could be the cause (Cantiello et al. 2009; Belkacem, Dupret & Noels 2010), but we do not have enough information to exclude other possibilities. For the moment we cannot firmly identify any specific cause of the observed spacings. EPIC 227552090 will not be viewed by *TESS* such that increasing the frequency resolution is not possible in the near future. Spectroscopic analysis of this star is a priority, as it will allow us to re-evaluate the information available from the *K2* light curve.

Future modelling of these particular stars will involve determining their the effective temperature and log g from snapshot spectroscopy. Unfortunately not all eight stars in the sample will be observed with *TESS* such that the light curves will not be extended and the frequency resolution will not improve in the near future. For those stars that will be observed, the additional data will be helpful to reconfirm the frequencies, and re-analyse *TESS* photometry merged with the *K2* photometry. None the less, our addition of *K2* high-frequency pulsators to the total number of upper main-sequence variable stars, and the large amplification soon by *TESS*, is bound to add incrementally to the much needed calibration of stellar evolution theory of hot massive stars. With *TESS*, massive star asteroseismology will certainly be getting a boost (Pedersen et al. 2019; Handler et al. 2019; Bowman et al. 2019a).

ACKNOWLEDGEMENTS

The research leading to these results has received funding from the European Research Council (ERC) under the European Union's Horizon 2020 research and innovation program (grant agreement no. 670519: MAMSIE). This research has made use of the SIMBAD data base, operated at CDS, Strasbourg, France. Some/all of the data presented in this paper were obtained from the MAST (STScI, Space Telescope Science Institute). STScI is operated by the Association of Universities for Research in Astronomy, Inc., under NASA contract NAS5-26555. This paper includes data collected by the *Kepler* mission. Funding for the *Kepler* mission is provided by the NASA Science Mission directorate.

REFERENCES

Aerts C., Rogers T. M., 2015, ApJ, 806, L33
Aerts C., Christensen-Dalsgaard J., Kurtz D. W., 2010, Asteroseismology. Springer, Heidelberg
Aerts C., Briquet M., Degroote P., Thoul A., van Hoolst T., 2011, A&A, 534, A98
Aerts C. et al., 2018a, ApJS, 237, 15
Aerts C. et al., 2018b, MNRAS, 476, 1234
Aerts C. et al., 2019a, A&A, 624, A75
Aerts C., Mathis S., Rogers T., 2019b, ARA&A, 57, 35
Aigrain S., Parviainen H., Pope B. J. S., 2016, MNRAS, 459, 2408
Andrae R. et al., 2018, A&A, 616, A8
Asplund M., Grevesse N., Sauval A. J., Scott P., 2009, ARA&A, 47, 481
Auvergne M. et al., 2009, A&A, 506, 411
Bailer-Jones C. A. L., Rybizki J., Fouesneau M., Mantelet G., Andrae R., 2018, AJ, 156, 58
Balona L. A., 2016, MNRAS, 457, 3724
Balona L. A. et al., 2011, MNRAS, 413, 2403
Baran A. S., Koen C., Pokrzywka B., 2015, MNRAS, 448, L16
Barnsley R. M., Steele I. A., 2013, A&A, 556, A81
Belkacem K. et al., 2009, Science, 324, 1540
Belkacem K., Dupret M. A., Noels A., 2010, A&A, 510, A6
Blomme R. et al., 2011, A&A, 533, A4
Borucki W. J. et al., 2010, Science, 327, 977
Bouabid M.-P., Dupret M.-A., Salmon S., Montalbán J., Miglio A., Noels A., 2013, MNRAS, 429, 2500
Bowman D. M., 2017, Amplitude Modulation of Pulsation Modes in Delta Scuti Stars. Springer Theses Series. ISBN 978-3-319-66649-5. Springer International Publishing, Basel
Bowman D. M., Kurtz D. W., Breger M., Murphy S. J., Holdsworth D. L., 2016, MNRAS, 460, 1970
Bowman D. M., Buysschaert B., Neiner C., Pápics P. I., Oksala M. E., Aerts C., 2018, A&A, 616, A77
Bowman D. M. et al., 2019a, Nat. Astron., 3, 760
Bowman D. M. et al., 2019b, A&A, 621, A135
Briquet M. et al., 2011, A&A, 527, A112
Buchler J. R., Goupil M. J., Serre T., 1995, A&A, 296, 405
Buysschaert B. et al., 2015, MNRAS, 453, 89
Buysschaert B., Neiner C., Martin A. J., Aerts C., Bowman D. M., Oksala M. E., Van Reeth T., 2018a, MNRAS, 478, 2777
Buysschaert B., Aerts C., Bowman D. M., Johnston C., Van Reeth T., Pedersen M. G., Mathis S., Neiner C., 2018b, A&A, 616, A148
Cantiello M. et al., 2009, A&A, 499, 279
de Jager C., Nieuwenhuijzen H., 1987, A&A, 177, 217
Degroote P. et al., 2009, A&A, 506, 111
Degroote P. et al., 2010, A&A, 519, A38
Deng L., Xiong D. R., 2001, MNRAS, 327, 881
Diago P. D. et al., 2009, A&A, 506, 125
Drilling J. S., Bergeron L. E., 1995, PASP, 107, 846
Dupret M.-A., Thoul A., Scuflaire R., Daszyńska-Daszkiewicz J., Aerts C., Bourge P.-O., Waelkens C., Noels A., 2004, A&A, 415, 251
Dziembowski W., 1977, Acta Astron., 27, 203
Dziembowski W. A., Pamiatnykh A. A., 1993, MNRAS, 262, 204
Dziembowski W. A., Moskalik P., Pamyatnykh A. A., 1993, MNRAS, 265, 588
Fitzpatrick E. L., 1999, PASP, 111, 63
Frost E. B., 1902, ApJ, 15,
Gaia Collaboration et al., 2016, A&A, 595, A1
Gaia Collaboration et al., 2018, A&A, 616, A1
Gautschy A., Saio H., 1993, MNRAS, 262, 213
Green G. M. et al., 2018, MNRAS, 478, 651
Gutiérrez-Soto J. et al., 2009, A&A, 506, 133
Handler G. et al., 2004, MNRAS, 347, 454

Handler G. et al., 2006, MNRAS, 365, 327
Handler G. et al., 2019, ApJ, 874, L4
Hohle M. M., Neuhäuser R., Schutz B. F., 2010, Astron. Nachr., 331, 349
Houk N., Smith-Moore M., 1988, Michigan Catalogue of Two-dimensional Spectral Types for the HD Stars. Volume 4, Declinations -26.0 to -12.0. Univ. Michigan, Ann Arbor, MI
Howell S. B. et al., 2014, PASP, 126, 398
Huat A.-L. et al., 2009, A&A, 506, 95
Huber D. et al., 2016, ApJS, 224, 2
Jaschek M., Egret D., 1982, in Jaschek M., Groth H. G., eds, IAU Symp. Vol. 98, Be Stars, Kluwer, Dordrecht, p. 261
Johnston C., Tkachenko A., Aerts C., Molenberghs G., Bowman D. M., Pedersen M. G., Buysschaert B., Pápics P. I., 2019, MNRAS, 482, 1231
Kiriakidis M., El Eid M. F., Glatzel W., 1992, MNRAS, 255, 1P
Kurtz D. W., Shibahashi H., Murphy S. J., Bedding T. R., Bowman D. M., 2015, MNRAS, 450, 3015
Lenz P., Breger M., 2004, in Zverko J., Ziznovsky J., Adelman S. J., Weiss W. W., eds, IAU Symp. Vol. 224, The A-Star Puzzle. Kluwer, Dordrecht, p. 786
Lomb N. R., 1976, Ap&SS, 39, 447
Loumos G. L., Deeming T. J., 1978, Ap&SS, 56, 285
MacConnell D. J., 1981, A&AS, 44, 387
Maeder A., 2009, Physics, Formation and Evolution of Rotating Stars. Springer, Berlin Heidelberg
McCall M. L., 2004, AJ, 128, 2144
McNamara B. J., Jackiewicz J., McKeever J., 2012, AJ, 143, 101
Miglio A., Montalbán J., Dupret M.-A., 2007, Commun. Asteroseismol., 151, 48
Miglio A., Montalbán J., Noels A., Eggenberger P., 2008, MNRAS, 386, 1487
Moravveji E., 2016, MNRAS, 455, L67
Moravveji E., Aerts C., Pápics P. I., Triana S. A., Vandoren B., 2015, A&A, 580, A27
Moravveji E., Townsend R. H. D., Aerts C., Mathis S., 2016, ApJ, 823, 130
Moskalik P., Dziembowski W. A., 1992, A&A, 256, L5
Nassau J. J., Stephenson C. B., 1960, ApJ, 132, 130
Negueruela I., Steele I. A., Bernabeu G., 2004, Astron. Nachr., 325, 749
Neiner C. et al., 2009, A&A, 506, 143
Neiner C. et al., 2012, A&A, 546, A47
Ouazzani R.-M., Salmon S. J. A. J., Antoci V., Bedding T. R., Murphy S. J., Roxburgh I. W., 2017, MNRAS, 465, 2294
Pamyatnykh A. A., 1999, AcA, 49, 119
Pápics P. I., 2012, Astron. Nachr., 333, 1053
Pápics P. I. et al., 2012, A&A, 542, A55
Pápics P. I. et al., 2017, A&A, 598, A74
Paxton B., Bildsten L., Dotter A., Herwig F., Lesaffre P., Timmes F., 2011, ApJS, 192, 3
Paxton B. et al., 2013, ApJS, 208, 4
Paxton B. et al., 2015, ApJS, 220, 15
Paxton B. et al., 2018, ApJS, 234, 34
Pedersen M. G., Aerts C., Pápics P. I., Rogers T. M., 2018, A&A, 614, A128
Pedersen M. G. et al., In preparation
Pedersen M. G. et al., 2019, ApJ, 872, L9
Pigulski A., Pojmański G., 2008, A&A, 477, 917
Porter J. M., Rivinius T., 2003, PASP, 115, 1153
Ricker G. R. et al., 2014, Proceedings of the SPIE , 9143, 914320
Rodríguez E., Breger M., 2001, A&A, 366, 178
Saio H. et al., 2007, ApJ, 654, 544
Salaris M., Cassisi S., 2017, R. Soc. Open Sci., 4, 170192
Scargle J. D., 1982, ApJ, 263, 835
Schwarzenberg-Czerny A., 2003, in Sterken C., ed., ASP Conf. Ser. Vol. 292, Interplay of Periodic, Cyclic and Stochastic Variability in Selected Areas of the H-R Diagram. Astron. Soc. Pac., San Francisco, p. 383
Stankov A., Handler G., 2005, ApJS, 158, 193
Steele I. A., Negueruela I., Clark J. S., 1999, A&AS, 137, 147
Szewczuk W., Daszyńska-Daszkiewicz J., 2017, MNRAS, 469, 13
Szewczuk W., Daszyńska-Daszkiewicz J., 2018, MNRAS, 478, 2243
Tassoul M., 1980, ApJS, 43, 469
Van Reeth T. et al., 2015, ApJS, 218, 27
Van Reeth T., Tkachenko A., Aerts C., 2016, A&A, 593, A120
Van Reeth T. et al., 2018, A&A, 618, A24
Vanderburg A., Johnson J. A., 2014, PASP, 126, 948
Vijapurkar J., Drilling J. S., 1993, ApJS, 89, 293
Waelkens C., 1991, A&A, 246, 453
Walczak P., Fontes C. J., Colgan J., Kilcrease D. P., Guzik J. A., 2015, A&A, 580, L9
White T. R. et al., 2017, MNRAS, 471, 2882

APPENDIX A: FREQUENCY LISTS

This appendix contains all the frequency lists extracted by pre-whitening described in Section 2.4. The first column reads the

Table A1. Frequency list for EPIC 202691120 extracted by pre-whitening. The standard deviation of the residuals is: 0.063 mmag.

ID	Frequency (d^{-1})	Amplitude (mmag)	SN	Notes
ν_1	9.4112(2)	8.3(3)	25.2	
ν_2	7.9107(2)	6.7(2)	28.5	
ν_3	0.3419(5)	2.3(2)	12.5	
ν_4	8.5187(6)	2.1(2)	16.1	
ν_5	8.9612(7)	1.7(2)	15.0	
ν_6	2.2919(7)	1.6(2)	9.8	
ν_7	0.0925(9)	1.1(1)	7.7	
ν_8	7.480(1)	1.0(1)	10.6	
ν_9	6.883(1)	0.9(1)	9.3	
ν_{10}	1.307(1)	0.8(1)	5.8	
ν_{11}	1.126(1)	0.7(1)	5.3	
ν_{12}	0.986(1)	0.7(1)	5.3	$\nu_6 - \nu_{10}$
ν_{13}	1.088(1)	0.7(1)	5.0	$\nu_{12} - \nu_7$

Table A2. Frequency list for EPIC 202929357 extracted by pre-whitening. The standard deviation of the residuals is: 0.070 mmag. No combinations were found.

ID	Frequency (d^{-1})	Amplitude (mmag)	SN	Notes
ν_1	9.1640(4)	4.8(2)	17.4	
ν_2	10.8271(4)	4.7(2)	14.3	
ν_3	13.0969(6)	3.2(2)	15.3	
ν_4	8.0155(5)	3.2(2)	14.6	
ν_5	10.4413(5)	3.1(2)	13.8	
ν_6	8.7579(5)	2.6(2)	13.9	
ν_7	9.5796(6)	2.2(1)	12.4	
ν_8	10.1467(6)	2.1(2)	11.4	
ν_9	7.8876(5)	2.1(1)	15.3	
ν_{10}	12.4737(6)	1.9(1)	12.4	
ν_{11}	11.4182(8)	1.3(1)	8.6	
ν_{12}	8.8193(8)	1.3(1)	11.2	
ν_{13}	9.4718(8)	1.3(1)	10.6	
ν_{14}	11.952(1)	1.0(1)	7.4	
ν_{15}	4.0458(9)	1.0(1)	6.0	
ν_{16}	0.051(1)	0.9(1)	6.6	
ν_{17}	9.063(1)	0.7(1)	7.2	
ν_{18}	8.861(1)	0.7(1)	7.3	
ν_{19}	10.076(1)	0.7(1)	6.3	
ν_{20}	12.526(1)	0.7(1)	5.5	
ν_{21}	13.723(1)	0.7(1)	5.6	
ν_{22}	7.456(1)	0.6(1)	6.6	
ν_{23}	11.265(1)	0.6(1)	5.4	

Table A3. Frequency list for EPIC 223832867 extracted by pre-whitening. The standard deviation of the residuals is: 0.065 mmag. Modes identified by Pigulski & Pojmański (2008) are marked with PP08, with their amplitude in mmag between brackets.

ID	Frequency (d^{-1})	Amplitude (mmag)	SN	Notes
ν_1	5.5708(5)	8.4(5)	22.1	PP08 (8.6)
ν_2	5.1640(4)	8.0(4)	24.4	PP08 (12.0)
ν_3	5.1182(5)	6.9(4)	22.7	PP08 (13.9)
ν_4	4.9407(4)	5.4(3)	27.9	PP08 (6.6)
ν_5	0.3949(6)	2.3(2)	14.3	$\nu_1 - \nu_2$
ν_6	7.1117(7)	1.7(2)	12.3	
ν_7	0.3657(6)	1.8(1)	11.8	
ν_8	7.719(1)	1.0(1)	7.0	
ν_9	3.690(1)	0.9(1)	7.5	
ν_{10}	0.597(1)	1.0(1)	6.9	
ν_{11}	6.501(1)	0.7(1)	6.0	
ν_{12}	3.124(1)	0.7(1)	5.9	
ν_{13}	8.487(1)	0.6(1)	5.5	
ν_{14}	0.690(1)	0.6(1)	5.1	
ν_{15}	7.045(1)	0.6(1)	5.1	

Table A4. Frequency list for EPIC 227552090 extracted by pre-whitening. The standard deviation of the residuals is: 0.048 mmag.

ID	Frequency (d^{-1})	Amplitude (mmag)	SN	Notes
ν_1	5.3131(2)	7.0(2)	33.2	
ν_2	6.0599(4)	2.8(2)	17.4	
ν_3	6.1849(6)	1.9(1)	13.0	
ν_4	0.4907(6)	1.7(1)	15.6	
ν_5	6.3551(7)	1.5(1)	11.0	
ν_6	7.5387(7)	1.4(1)	11.5	
ν_7	6.5310(7)	1.3(1)	10.9	$\nu_2 + \nu_4$
ν_8	5.4690(7)	1.2(1)	11.4	
ν_9	6.4452(8)	1.1(1)	10.2	
ν_{10}	7.4972(9)	0.9(1)	10.2	
ν_{11}	0.0302(7)	0.88(8)	5.9	
ν_{12}	7.450(1)	0.8(1)	7.9	
ν_{13}	8.008(1)	0.7(1)	7.2	
ν_{14}	6.627(1)	0.7(1)	7.2	
ν_{15}	7.188(1)	0.64(9)	7.3	
ν_{16}	5.800(1)	0.62(9)	7.3	$\nu_1 + \nu_4$
ν_{17}	6.149(1)	0.60(9)	6.9	
ν_{18}	5.644(1)	0.54(9)	6.8	
ν_{19}	10.782(1)	0.47(8)	7.0	
ν_{20}	8.831(1)	0.45(8)	5.7	
ν_{21}	8.185(2)	0.43(8)	5.4	
ν_{22}	10.628(2)	0.43(8)	6.9	$2\nu_1$
ν_{23}	0.108(1)	0.42(8)	5.2	
ν_{24}	0.338(2)	0.39(8)	5.2	

assigned ID of each pre-whitened frequency, the second column the frequency with the error on the last figure between brackets, the third column the corresponding amplitude with the error on the last figure between brackets, and the fourth column the S/N of that peak. Finally, the fifth column denotes any identified combinations/harmonics. In Table A3, the column is also used to identify peaks found previously by Pigulski & Pojmański (2008) for EPIC 223832867.

Table A5. Frequency list for EPIC 233986359 extracted by pre-whitening. The standard deviation of the residuals is: 0.1606 mmag.

ID	Frequency (d^{-1})	Amplitude (mmag)	SN	Notes
ν_1 (fg1)	2.7057(5)	8.2(5)	19.7	
ν_2 (fg1)	2.7495(4)	7.1(4)	18.6	
ν_3 (fg2)	5.6519(9)	3.4(4)	14.0	
ν_4 (fg2)	5.7137(9)	3.1(4)	12.8	
ν_5 (fg0)	0.066(1)	2.4(3)	9.1	$\nu_3 - \nu_4$
ν_6 (fg2)	5.267(1)	2.3(3)	9.0	
ν_7 (fg2)	5.381(1)	2.3(3)	7.9	
ν_8 (fg2)	5.417(1)	2.0(3)	8.0	$2\nu_1$
ν_9 (fg0)	0.043(1)	1.9(3)	5.3	$\nu_2 - \nu_1$
ν_{10} (fg0)	0.132(1)	1.7(3)	5.6	$2\nu_5$
ν_{11} (fg2)	5.327(2)	1.6(3)	7.1	
ν_{12} (fg2)	5.134(2)	1.6(3)	6.7	
ν_{13} (fg1)	3.088(1)	1.5(3)	5.2	

Table A6. Frequency list for EPIC 235094159 extracted by pre-whitening. The standard deviation of the residuals is 0.085 mmag.

ID	Frequency (d^{-1})	Amplitude (mmag)	SN	Notes
ν_1	9.3090(1)	21.3(3)	47.1	
ν_2	8.7557(3)	7.7(3)	28.9	
ν_3	0.0381(4)	5.0(3)	15.9	
ν_4	11.9416(6)	3.7(3)	16.4	
ν_5	9.1468(5)	3.2(2)	14.8	
ν_6	0.0838(6)	2.6(2)	9.6	$2\nu_3$
ν_7	6.5384(6)	2.5(2)	15.3	
ν_8	11.4840(7)	2.2(2)	10.8	
ν_9	9.5727(8)	1.9(2)	10.1	
ν_{10}	0.1073(8)	1.7(2)	7.7	$3\nu_3$
ν_{11}	7.3560(9)	1.5(2)	9.9	
ν_{12}	8.7034(9)	1.5(2)	9.1	
ν_{13}	13.672(1)	1.3(2)	9.0	
ν_{14}	10.299(1)	1.3(2)	7.5	
ν_{15}	10.927(1)	1.3(2)	7.6	
ν_{16}	1.918(1)	1.2(2)	7.1	
ν_{17}	13.290(1)	1.1(2)	7.8	
ν_{18}	1.562(1)	1.0(2)	6.2	
ν_{19}	16.568(1)	1.0(2)	9.6	
ν_{20}	9.362(1)	1.0(1)	6.4	
ν_{21}	8.099(1)	0.9(2)	7.2	
ν_{22}	8.232(1)	0.9(1)	6.9	
ν_{23}	4.362(1)	0.9(1)	7.9	
ν_{24}	12.776(1)	0.9(1)	6.8	
ν_{25}	14.736(1)	0.9(1)	7.9	
ν_{26}	9.125(1)	0.9(1)	6.3	
ν_{27}	11.898(1)	0.9(1)	6.3	
ν_{28}	0.215(1)	0.8(1)	5.5	
ν_{29}	1.293(1)	0.8(1)	5.5	
ν_{30}	1.045(1)	0.8(1)	5.6	
ν_{31}	12.411(1)	0.8(1)	6.4	
ν_{32}	0.350(1)	0.8(1)	5.4	$9\nu_3$
ν_{33}	0.304(1)	0.8(1)	5.3	$8\nu_3$
ν_{34}	0.938(1)	0.8(1)	5.2	
ν_{35}	10.582(1)	0.7(1)	5.7	

Table A7. Frequency list for EPIC 235151005 extracted by pre-whitening. The standard deviation of the residuals is 0.032 mmag.

ID	Frequency (d^{-1})	Amplitude (mmag)	SN	Notes
ν_1 (fg2)	3.3812(3)	3.7(2)	31.6	$\nu_4+\nu_{15}$, $\nu_3+\nu_{15}$
ν_2 (fg2)	3.1203(8)	1.6(2)	15.1	$2\nu_9$, $\nu_{11}+\nu_{16}$
ν_3 (fg1)	1.9134(7)	1.54(1)	14.3	
ν_4 (fg1)	1.884(1)	1.0(1)	11.3	
ν_5 (fg2)	3.152(1)	0.9(1)	10.1	
ν_6 (fg2)	3.030(1)	0.8(1)	9.2	$\nu_9+\nu_{16}$
ν_7 (fg0)	0.031(1)	0.8(1)	9.1	$\nu_3-\nu_4$, $\nu_{15}-\nu_{16}$
ν_8 (fg2)	3.182(1)	0.7(1)	9.3	
ν_9 (fg1)	1.565(1)	0.7(1)	9.1	$1/2\nu_2$
ν_{10} (fg0)	0.302(1)	0.6(1)	7.5	
ν_{11} (fg1)	1.635(1)	0.56(9)	7.5	
ν_{12} (fg0)	0.352(1)	0.54(9)	7.7	$\nu_3-\nu_9$
ν_{13} (fg2)	3.333(2)	0.42(9)	7.2	
ν_{14} (fg2)	3.797(2)	0.40(8)	6.3	$\nu_3+\nu_4$
ν_{15} (fg1)	1.496(2)	0.39(8)	5.6	
ν_{16} (fg1)	1.470(2)	0.38(8)	5.9	
ν_{17} (fg2)	3.411(2)	0.35(7)	5.8	$\nu_3+\nu_{15}$
ν_{18} (fg2)	3.826(2)	0.34(8)	6.0	$2\nu_3$
ν_{19} (fg0)	0.219(2)	0.31(7)	5.0	
ν_{20} (fg2)	3.492(2)	0.30(7)	5.3	$\nu_3+\nu_9$
ν_{21} (fg2)	3.056(2)	0.29(7)	5.0	$\nu_9+\nu_{15}$

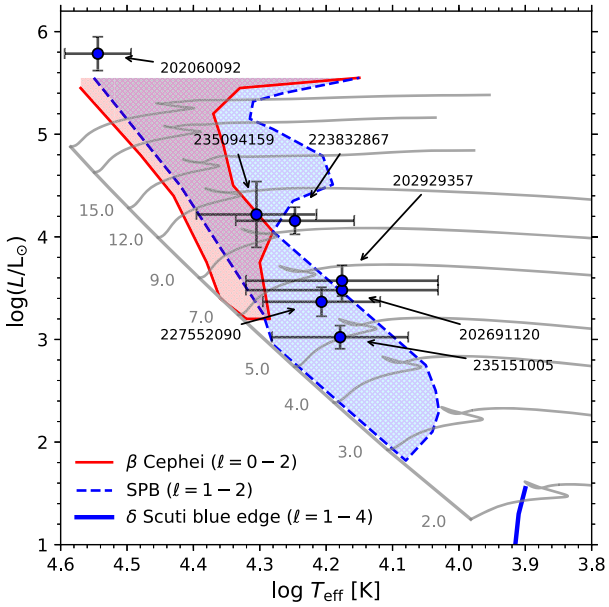

Figure B1. Theoretical HRD using effective temperatures from de Jager & Nieuwenhuijzen (1987) and luminosities derived using *Gaia* DR2 and the statistical model by Pedersen et al. (2019a).The grey evolutionary tracks are by Johnston et al. (2019), the massive star instability strips from Walczak et al. (2015), and the δ Scuti blue edge is from Dupret et al. (2004).

APPENDIX B: *GAIA*

In this appendix, we summarize the *Gaia* data used for the CMD in Fig. 11 in Table B1. The last three columns are values from Bailer-Jones et al. (2018). To confirm the validity of the diagram in Fig. 11, we use approximate estimates of the effective temperature from spectral type and the *Gaia*-DR2 parameters to derive the luminosities. We follow the method of Pedersen et al. (in prep.) to achieve this and provide only a summary.

The method starts from the observed apparent magnitudes in different filters and applies bolometric corrections,

$$m_{\rm bol} = m_{S_\lambda} + BC_{S_\lambda} - A_{S_\lambda}, \tag{B1}$$

with $m_{\rm bol}$ the apparent bolometric magnitude, m_{S_λ} the apparent magnitude measured in photometric passband with transmission curve S_λ, and BC_{S_λ} and A_{S_λ} the bolometric correction and extinction for this transmission curve S_λ. Bolometric corrections BC_{S_λ} have been computed for *Gaia* passbands but are restricted to the temperature range of $T_{\rm eff} \in [2600\text{–}8000\,{\rm K}]$ (see e.g. Andrae et al. 2018). Therefore, Pedersen et al. (in prep.) computed BC_{S_λ} for the temperature regime relevant for SPB and β Cep stars.

The extinction values A_{S_λ} are procured from the reddening values $E(B-V)$ of each individual star and the reddening law,

$$A_{S_\lambda} = R_{S_\lambda} E(B-V), \tag{B2}$$

with R_{S_λ} the ratio of total to selective reddening in the passband with transmission S_λ. Pedersen et al. (in prep.) obtain $E(B-V)$ from 3D dust maps by Green et al. (2018), and derive R_{S_λ} versus λ using the York's extinction solver (McCall 2004) assuming the Fitzpatrick (1999) reddening law. This finally yields the apparent bolometric magnitude $m_{\rm bol}$ for each star.

Using the distances from *Gaia* DR2 (Gaia Collaboration et al. 2016, 2018), see Table B1, as calculated by Bailer-Jones et al. (2018), the luminosities are then retrieved through,

$$\log\, L_\star/L_\odot = -0.4(m_{\rm bol} - 5\log\, d + 5 - M_{\rm bol,\odot}), \tag{B3}$$

where d is the distance measured in parsec and $M_{\rm bol,\odot}$ the absolute bolometric magnitude of the Sun.

The lack of availability of spectroscopy forces us to derive the effective temperatures from spectral type-effective temperature calibrations, e.g. as provided by de Jager & Nieuwenhuijzen (1987) for B-type stars. The authors of this work collected the most recent and complete (in their time) sets of tabular values of effective temperature and spectral type. The sets were then used to derive relations where $\log T_{\rm eff}$ and $\log L_\star$ are written as Chebyhev polynomials depending on two continuous analytical variables s (connected to spectral class) and b (connected to luminosity class), such that $\log T_{\rm eff}(s,b)$ and $\log L_\star(s,b)$. The authors provided tables from which, given a spectral type and luminosity class, the effective temperature is procured. The 1σ, which is 0.012 per unit weight for $\log T_{\rm eff}$, is given as the approximate error on any $\log T_{\rm eff}$ derived from the spectral type (de Jager & Nieuwenhuijzen 1987). This is the uncertainty that we will also use.

For EPIC 202060092, estimates of the effective temperature and surface gravity are provided by Buysschaert et al. (2015) so we use those values instead. For EPIC 20269110 and EPIC 202929357, the spectral type classification was assigned OB$^-$ by Drilling & Bergeron (1995). We noted in Section 3.2 that in their scheme, OB was assigned to anything that appears earlier than B6 but that late B-type or early A-type supergiants may imitate OB behaviour (Nassau & Stephenson 1960). This covers a large range in temperatures and luminosities. To cover the extreme case that the stars may be late B-type or early A we assume $T_{\rm eff} = 15000 \pm 5000$ K which covers the mid to late B range. For all stars, expect EPIC 202060092, we assume a surface gravity $\log g = 4.0 \pm 0.5$, which approximately reflects the main sequence in this mass range. We summarize the relevant parameters in Table B2. The errors on

Table B1. *Gaia*-DR2 values for the stars in our sample retrieved from http://gea.esac.esa.int/archive/. The last three columns are distances from Bailer-Jones et al. (2018). EPIC 233986359 is not in *Gaia* DR2 and therefore not included in the table.

EPIC ID	*Gaia* ID	G mean mag. (mag)	G absorption (mag)	BP−RP (mag)	E(BP−RP) (mag)	Parallax (arcsec)	Distance (pc)	Lower bound (pc)	Upper bound (pc)
202060092	3377246313718987392	8.956	1.676	0.806	0.872	0.517	1832.7	1675.4	2021.7
202691120	6032148702447357952	10.232	1.256	0.425	0.640	0.512	1862.6	1708.9	2046.0
202929357	6042284859603154944	10.873	NA*	0.236	NA*	0.333	2790.2	2410.0	3306.1
223832867	4065715861804605696	8.900	1.407	0.532	0.680	0.698	1392.5	1265.5	1547.3
227552090	4096294139196441216	9.752	1.338	0.491	0.674	0.701	1389.0	1246.0	1568.1
235094159	4112611952506129408	12.369	1.147	0.501	0.579	0.126	6000.2	4451.2	8673.5
235151005	4111320477373506304	8.642	1.651	0.621	0.835	2.277	435.3	416.4	456.1

Note: * indicates that the extinction in the *G* band is poorly estimated and the value untrustworthy (Andrae et al. 2018).

Table B2. Assumed stellar parameters, reddening values, and derived luminosities following using the model by Pedersen et al. (inprep.).

EPIC ID	SpT	log $T_{\rm eff}$ (K)	log g (cm s^{-2})	$E(B-V)$ Green et al. (2018)	log L ($L_\odot$)
202060092[1]	O9V:p	4.5 ± 0.1	4.5 ± 0.5	1.22 ± 0.02	6.0 ± 0.2
202691120[2]	OB$^-$	4.2 ± 0.1	4.0 ± 0.5	0.47 ± 0.01	3.5 ± 0.1
202929357[2]	OB$^-$	4.2 ± 0.1	4.0 ± 0.5	0.44 ± 0.00001	3.6 ± 0.2
223832867	B2Ib/II	4.3 ± 0.1	4.0 ± 0.5	0.60 ± 0.01	4.2 ± 0.1
227552090	B3Ib	4.2 ± 0.1	4.0 ± 0.5	0.33 ± 0.01	3.3 ± 0.1
235094159	B2III	4.3 ± 0.1	4.0 ± 0.5	0.62 ± 0.13	4.2 ± 0.3
235151005	B5III	4.2 ± 0.1	4.0 ± 0.5	0.56 ± 0.0008	3.0 ± 0.1

Notes: (1) Values from Buysschaert et al. (2015).
(2) The spectral type classification is vague, therefore the temperature cannot be retrieved from de Jager & Nieuwenhuijzen (1987).

the luminosity are derived by means of error propagation from the uncertainty on the distance, and temperature, as well as bolometric correction. See Pedersen et al. (in prep.) for details.

The final results of this exercise are summarized in Fig. B1. On this figure, we show the positions of the stars in terms of luminosity and effective temperature. For illustrative purposes, we include evolutionary tracks computed by Johnston et al. (2019) with the MESA stellar evolution code (Paxton et al. 2011, 2013, 2015, 2018). These are non-rotating tracks with $Z = 0.014$, an initial hydrogen abundance $X_{\rm ini} = 0.71$, diffuse exponential overshooting parameter $f_{\rm ov} = 0.020$, the Asplund et al. (2009) heavy element mixture, and the standard MESA opacity tables that incorporate different sources (Paxton et al. 2011). Additionally, we include two approximate instability strips: the β Cephei and SPB instability regions, as computed by Walczak et al. (2015). These were calculated using a combination of the MESA stellar evolution code and the Dziembowski linear, non-adiabatic pulsation code (Dziembowski 1977), for $Z = 0.015$, $X_{\rm ini} = 0.70$, exponential overshooting parameter $f_{\rm ov} = 0.020$, the Asplund et al. (2009) solar mixture, and OPAL opacity tables. We also include the δ Scuti blue edge for $\ell = 1-4$ from Dupret et al. (2004), for solar metallicity. We emphasize that the strips and the blue δ Scuti edge are included to guide the eye, and are not meant as a comparison between theory and observations. The β Cep strip is sensitive to many parameters, i.e. metallicity, given that the modes are excited by a heat mechanism (Szewczuk & Daszyńska-Daszkiewicz 2017).

The relative positions of the stars are very similar to the positions in Fig. 11, demonstrating that the CMD is a suitable proxy for the theoretical HRD whenever spectroscopic parameters are not available. The error bars on the temperatures are high, as expected, and this is also propagated into the luminosity. Fig. B1 indicates that the stars are most likely unstable to low- and/or high-frequency oscillations.

This paper has been typeset from a TEX/LATEX file prepared by the author.